Unitary model for the $\gamma p \to \gamma \pi^0 p$ reaction and the magnetic dipole moment of the $\Delta^+(1232)$

Wen-Tai Chiang,[1,2] M. Vanderhaeghen,[3,4] Shin Nan Yang,[1] and D. Drechsel[5]
[1]*Department of Physics and National Center for Theoretical Sciences at Taipei, National Taiwan University, Taipei 10617, Taiwan*
[2]*Institute of Physics, Academia Sinica, Taipei 11529, Taiwan*
[3]*Jefferson Laboratory, Newport News, Virginia 23606*
[4]*Department of Physics, College of William and Mary, Williamsburg, Virginia 23187*
[5]*Institut für Kernphysik, Universität Mainz, D-55099 Mainz, Germany*
(Received 8 September 2004; published 21 January 2005)

Radiative pion photoproduction in the $\Delta(1232)$-resonance region is studied with the aim of accessing the $\Delta^+(1232)$ magnetic dipole moment. We present a unitary model of the $\gamma p \to \gamma \pi N$ ($\pi N = \pi^0 p,\ \pi^+ n$) reactions, where the πN rescattering is included in an onshell approximation. In this model, the low-energy theorem which couples the $\gamma p \to \gamma \pi N$ process in the limit of a soft final photon to the $\gamma p \to \pi N$ process is exactly satisfied. We study the sensitivity of the $\gamma p \to \gamma \pi^0 p$ process at higher values of the final photon energy to the $\Delta^+(1232)$ magnetic dipole moment. We compare our results with existing data and give predictions for forthcoming measurements of angular and energy distributions. It is found that the photon asymmetry and a helicity cross section are particularly sensitive to the Δ^+ magnetic dipole moment.

DOI: 10.1103/PhysRevC.71.015204 PACS number(s): 12.39.Jh, 13.60.Fz, 14.20.Gk

I. INTRODUCTION

The $\Delta(1232)$ is the first and most prominent excited state of the nucleon and the only well isolated nucleon resonance. Its properties provide an important test for theoretical descriptions in the nonperturbative domain of Quantum Chromo Dynamics (QCD). There are two kinds of electromagnetic properties of the Δ. The first one involves the $N \to \Delta$ transition, described by the magnetic dipole ($\mu_{N\Delta}$) and electric quadrupole ($Q_{N\Delta}$) transition moments to be determined from pion electromagnetic production [1,2]. The other properties involve the Δ itself, the magnetic dipole moment μ_Δ, the electric quadrupole moment Q_Δ, and the magnetic octupole moment of the resonance. They are difficult to measure because of the short lifetime of the Δ.

In particular, the magnetic dipole moment (MDM) of the $\Delta(1232)$ is of considerable theoretical interest. In symmetric SU(6) quark models, the nucleon and the Δ resonance are degenerate and their magnetic moments are related through $\mu_\Delta = e_\Delta\, \mu_p$, where e_Δ is the electric charge of the Δ, and μ_p is the proton magnetic moment. However, different theoretical models predict considerable deviations from this SU(6) value [3]. The $\Delta(1232)$ MDM has also been investigated on the lattice at rather large quark masses [4], and very recently the chiral extrapolation of the $\Delta(1232)$ MDM, including the next-to-leading nonanalytic variation with the quark mass, was also studied [5]. At present, there still is a considerably large gap in quark mass to bridge between the state-of-the-art lattice QCD calculations and the chiral limit. Therefore, it would be extremely helpful to know the resonance MDM for the physical quark mass values, through experiment. Unfortunately, experimental information on the MDMs beyond the ground state baryon octet is very scarce. With the notable exception of the Ω^- baryon, these higher nucleon resonances decay strongly and thus have lifetimes too short to measure their MDMs in the conventional way through spin precession measurements.

The magnetic moment of the $\Delta^{++}(1232)$ has been measured by the reaction $\pi^+ p \to \gamma \pi^+ p$ [6,7]. As a result of these measurements, and using different theoretical analyses, the PDG [8] quotes the range $\mu_{\Delta^{++}} = 3.7 - 7.5\, \mu_N$ (where μ_N is the nuclear magneton), while SU(6) symmetry results in the value $\mu_{\Delta^{++}} = 5.58\, \mu_N$. The large uncertainty in the extraction of the experimental value is due to large nonresonant contributions to the $\pi^+ p \to \gamma \pi^+ p$ reaction because of bremsstrahlung from the charged pion (π^+) and proton (p).

For the $\Delta^+(1232)$, it has been proposed [9] to determine its magnetic moment through measurement of the $\gamma p \to \gamma \pi^0 p$ reaction. Due to the small cross sections for this reaction, which is proportional to $\alpha_{em}^2 = 1/(137)^2$, a first measurement has only recently been reported by the A2/TAPS collaboration at MAMI [10]. At present, dedicated experiments are being performed with much higher count rates by using 4π detectors, such as the Crystal Ball detector at MAMI [11]. The analysis of this next generation of dedicated experiments requires a substantial theoretical effort aimed at minimizing the model dependencies in the extraction of the Δ^+ MDM from the measurement of the $\gamma p \to \gamma \pi^0 p$ observables.

First estimates for the reaction $\gamma p \to \gamma \pi^0 p$, including only the Δ-resonant mechanism, were performed in Refs. [12,13]. An improved calculation which contains both the Δ-resonant mechanism and a background of nonresonant contributions has subsequently been carried out in Ref. [14]. The starting point of the model is an effective Lagrangian description of the $\gamma p \to \pi^0 p$ process. Then an additional photon is coupled in a gauge-invariant way to describe the $\gamma p \to \gamma \pi^0 p$ reaction. The result is a tree level calculation with part of the final state interaction effects taken into account by the finite width of the Δ. This model was used in the analysis of the pioneering measurement of the $\gamma p \to \gamma \pi^0 p$ cross sections and an initial value of $\mu_{\Delta^+} = [2.7^{+1.0}_{-1.3}(\text{stat.}) \pm 1.5(\text{syst.}) \pm 3(\text{theor.})]\, \mu_N$ has been extracted in Ref. [10].

Although the tree-level model of Ref. [14] gives a qualitatively good description of the data of Ref. [10], a detailed quantitative comparison requires the inclusion of rescattering effects. Such rescattering effects were found to be important in the case of pion photoproduction (see, e.g., [15]). Since an accurate theoretical description of the reaction $\gamma p \to \gamma \pi^0 p$ is essential for extracting a precise value for μ_{Δ^+}, it is imperative to obtain an estimate of the effects of the final-state interaction to the best of our capability. It is therefore the aim of our present work to describe the radiative pion photoproduction by a properly unitarized theory.

We start in Sec. II by specifying the kinematics and cross section of the reaction $\gamma p \to \gamma \pi^0 p$. In Sec. III, we present a unitary model for the $\gamma p \to \pi^0 p$ process with a transition potential that is derived from an effective Lagrangian with Born terms and vector mesons exchange in addition to the Δ-excitation mechanism. Our model is very similar to MAID [16] in that only the onshell rescattering effects are included in the nonresonant multipoles. We further show a selection of our fits to various experimental data, which have been used to fix all the parameters of the strong interaction. Our model for the $\gamma\, p \to \gamma\, \pi^0\, p$ reaction in the $\Delta(1232)$-resonance region is described in Sec. IV. The transition potential for this reaction is given by all the tree diagrams that can be obtained from the effective Lagrangian previously adopted for the $\gamma p \to \pi^0 p$ process, with the addition of the anomaly terms generated from the $\pi^0 \to \gamma + \gamma$ vertex. We then proceed to estimate the final-state interaction effects by including the onshell rescattering between pion and nucleon. In Sec. V we compare our results for the $\gamma\, p \to \gamma\, \pi^0\, p$ reaction with the existing data. We further present our predictions for several angular and energy distributions as well as polarization observables that are expected to be measured in forthcoming experiments. In each case we demonstrate the sensitivity with respect to the $\Delta^+(1232)$ magnetic dipole moment. We close by summarizing our findings in Sec. VI.

II. KINEMATICS AND CROSS SECTION FOR THE $\gamma p \to \gamma \pi^0 p$ REACTION

In the $\gamma p \to \gamma \pi N$ process, a photon (k, λ) hits a proton target (p, s_N), leading to a final state with a photon (k', λ'), a pion (q), and a proton or neutron (p', s'_N). Here k, k', p, p', and q are the four momenta of the respective particles, λ and λ' denote the photon helicities, and s_N and s'_N are the nucleon spin projections.

Our results for the experimental observables will be expressed in the center-of-mass (c.m.) frame of the initial γp system with total c.m. energy squared given by the usual Mandelstam invariant $s = (k + p)^2$. The kinematics of the $\gamma p \to \gamma \pi N$ reaction can be described by 5 variables. First, we choose the energies E_γ and E'_γ of the initial and outgoing photon, respectively. The other three variables are the polar (θ_γ) and azimuthal (ϕ_γ) angles of the final photon, and θ_π, the polar angle of the pion. These angles are defined with regard to an x-z plane that contains the initial particles and the final pion, with the photon momentum $\boldsymbol{k}$ pointing in the z direction and $\phi_\pi \equiv 0$.

The unpolarized fivefold differential cross section for the $\gamma p \to \gamma \pi N$ reaction, differential with respect to the outgoing photon energy and angles as well as the pion angles in the c.m. system, takes the form

$$\left(\frac{d\sigma}{dE'_\gamma\, d\Omega'_\gamma\, d\Omega_\pi}\right)^{\text{c.m.}} = \frac{1}{(2\pi)^5}\,\frac{1}{32\sqrt{s}}\,\frac{E'_\gamma}{E_\gamma}\,\frac{|\boldsymbol{q}|^2}{|\boldsymbol{q}|(E'_N + \omega_q) + E'_\gamma \omega_q \cos\theta_{\gamma'\pi}} \times \left(\frac{1}{4}\sum_\lambda \sum_{s_N} \sum_{\lambda'} \sum_{s'_N} |\, \varepsilon_\mu(k,\lambda)\, \varepsilon^*_\nu(k',\lambda')\, \mathcal{M}^{\nu\mu}\, |^2\right). \tag{1}$$

Unless otherwise specified, E_γ and E'_γ refer to the initial and final photon energies in the c.m. system. Furthermore, ω_q and $\boldsymbol{q}$ denote the energy and momentum of the pion; E'_N denotes the final nucleon energy; $\theta_{\gamma'\pi}$ denotes the c.m. angle between the outgoing photon and the pion; and $\varepsilon_\mu(k,\lambda)$ and $\varepsilon^*_\nu(k',\lambda')$ are the polarization vectors of the incoming and outgoing photons, respectively. Furthermore, $\mathcal{M}^{\nu\mu}$ is a tensor for the $\gamma p \to \gamma \pi N$ process, which is discussed in Sec. IV.

We will also show results for partially integrated cross sections of the $\gamma p \to \gamma \pi^0 p$ reaction, e.g., the cross section $d\sigma/dE'_\gamma$ differential with respect to the outgoing photon c.m. energy, or the cross section $d\sigma/dE'_\gamma d\Omega_\pi^{\text{c.m.}}$ differential with respect to the outgoing photon c.m. energy and the pion c.m. solid angle. These cross sections are obtained by integrating the fully differential cross section of Eq. (1) over the appropriate part of the phase space.

III. UNITARY MODEL FOR THE $\gamma p \to \pi N$ REACTION

In the dynamical approach to pion photo- and electroproduction [17], where unitarity is built in by explicit inclusion of the final state πN interaction, the T matrix is expressed as

$$t_{\gamma\pi} = v_{\gamma\pi} + v_{\gamma\pi}\, g_0\, t_{\pi N}, \tag{2}$$

where $v_{\gamma\pi}$ is a transition operator for the reaction $\gamma N \to \pi N$, and $t_{\pi N}$ and g_0 denote the πN scattering matrix and the free propagator, respectively. If the onshell or K-matrix approximation is made, that is, the intermediate particles (pions and nucleons) are restricted to be on the mass shell, the magnitudes of the onshell momenta for the intermediate particles depend only on the total c.m. energy $W_{\pi N}$ of the $\gamma N \to \pi N$ process. We therefore obtain, as the expression for the physical amplitude in the c.m. frame,

$$t_{\gamma\pi}(\boldsymbol{q}, \boldsymbol{k}; W_{\pi N}) = v_{\gamma\pi}(\boldsymbol{q}, \boldsymbol{k}) - \frac{i}{32\pi^2}\,\frac{|\boldsymbol{q}|}{W_{\pi N}} \times \sum_{s'_N} \int d\Omega_{q'}\, T_{\pi N}(\boldsymbol{q}, -\boldsymbol{q}; \boldsymbol{q}', -\boldsymbol{q}')\, v_{\gamma\pi}(\boldsymbol{q}', \boldsymbol{k}), \tag{3}$$

where we sum over the final nucleon spins s'_N and the relevant πN channels. For example, in the case of $\gamma p \to \pi^0 p$ we need to include both $\pi^0 p$ and $\pi^+ n$ intermediate states. The Lorentz

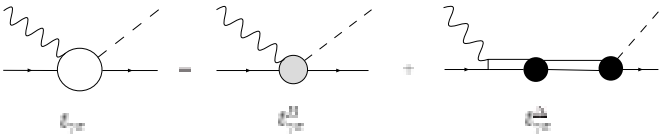

FIG. 1. Graphical representation of the pion photoproduction T matrix.

invariant T matrix is given by [18]

$$T_{\pi N}(\boldsymbol{q}', \boldsymbol{p}'; \boldsymbol{q}, \boldsymbol{p}) = \bar{u}(p', s'_N)\left[A + \tfrac{1}{2}(\not{q} + \not{q}')\, B\right] u(p, s_N), \tag{4}$$

where A and B are scalar functions of the invariants $s = W^2_{\pi N}$ and t, the square of the four-momentum transfer. We use the covariant normalization $\bar{u}u = 2M_N$ (M_N denotes the nucleon mass) for the Dirac spinors, and construct the functions A and B from the SAID partial wave amplitudes $f_{\ell\pm}(W_{\pi N})$.

For pion photoproduction in the $\Delta(1232)$-resonance region, the transition potential $v_{\gamma\pi}$ consists of two terms

$$v_{\gamma\pi} = v^B_{\gamma\pi} + v^\Delta_{\gamma\pi}, \tag{5}$$

where $v^\Delta_{\gamma\pi}$ corresponds to the resonance contribution $\gamma N \to \Delta \to \pi N$, and $v^B_{\gamma\pi}$ describes the background to be derived from an effective Lagrangian. The resulting T matrix can be decomposed into two terms (as shown in Fig. 1 [19]),

$$t_{\gamma\pi} = t^B_{\gamma\pi} + t^\Delta_{\gamma\pi}, \tag{6}$$

where

$$t^B_{\gamma\pi}(W_{\pi N}) = v^B_{\gamma\pi} + v^B_{\gamma\pi}\, g_0(W_{\pi N})\, t_{\pi N}(W_{\pi N}), \tag{7}$$

$$t^\Delta_{\gamma\pi}(W_{\pi N}) = v^\Delta_{\gamma\pi} + v^\Delta_{\gamma\pi}\, g_0(W_{\pi N})\, t_{\pi N}(W_{\pi N}). \tag{8}$$

The solid circles in Fig. 1 indicate that both the intermediate Δ states and the $\pi N \Delta$ vertices are dressed [20,21].

Applying Eq. (3) to the background contribution $t^B_{\gamma\pi}$, we obtain

$$t^B_{\gamma\pi}(\boldsymbol{q}, \boldsymbol{k}; W_{\pi N}) = v^B_{\gamma\pi}(\boldsymbol{q}, \boldsymbol{k}) - \frac{i}{32\pi^2}\frac{|\boldsymbol{q}|}{W_{\pi N}} \times \sum_{s'_N} \int d\Omega_{q'} T_{\pi N}(\boldsymbol{q}, -\boldsymbol{q}; \boldsymbol{q}', -\boldsymbol{q}')\, v^B_{\gamma\pi}(\boldsymbol{q}', \boldsymbol{k}). \tag{9}$$

Due to the onshell approximation, the multipole amplitudes $t^{B,\alpha}_{\gamma\pi}$, for the partial wave α, in Eq. (9), take the form

$$t^{B,\alpha}_{\gamma\pi} = v^{B,\alpha}_{\gamma\pi}\, \cos\,\delta_\alpha\, e^{i\delta_\alpha}, \tag{10}$$

where δ_α is the phase shift for πN scattering in the respective partial wave α.

The resonance structure $t^\Delta_{\gamma\pi}(E)$, as depicted in Fig. 1, is approximated by

$$t^\Delta_{\gamma\pi} = v^\Delta_{\gamma\pi}\left(M_\Delta \to M_\Delta - \frac{i}{2}\Gamma_\Delta\right) e^{i\phi(W_{\pi N})}, \tag{11}$$

with the phase $\phi(W_{\pi N})$ adjusted such that the Δ multipole amplitudes (M^Δ_{1+}, E^Δ_{1+}) carry the phase of the πN scattering phase $\delta_{33}(W_{\pi N})$ to ensure that the Fermi-Watson theorem is fulfilled. We further adopt the "complex mass scheme" by substituting $M_\Delta \to M_\Delta - \frac{i}{2}\Gamma_\Delta$ with an energy independent width Γ_Δ, as was suggested by Refs. [14,22,29] in order

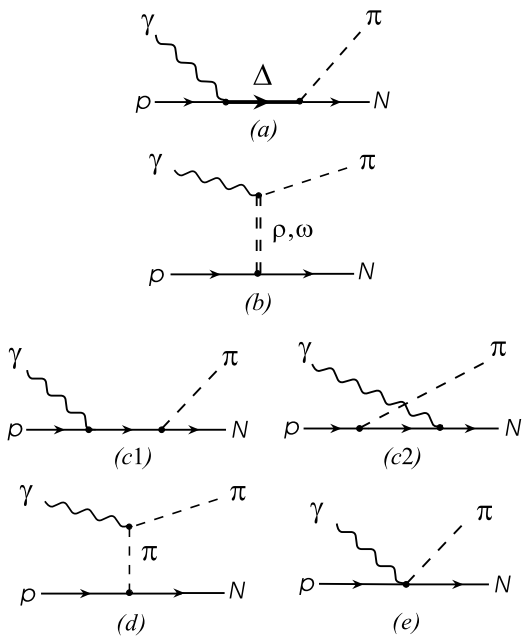

FIG. 2. Diagrams for the $\gamma p \to \pi N$ reaction in the $\Delta(1232)$ region: Δ resonance excitation (a), vector meson exchange (b), nucleon pole terms (c1-c2), pion pole term (d), and Kroll-Rudermann term (e).

to maintain the gauge invariance of the Δ contribution to the $\gamma N \to \gamma\pi N$ reaction. Since the background contribution of Eq. (10) satisfies the Fermi-Watson theorem separately, the total multipole amplitude will also carry the proper πN phase.

In this work we focus on the energy region of the $\Delta(1232)$ resonance and neglect the contribution from the higher resonances. Although this is an excellent approximation close to the $\Delta(1232)$ region, it is inevitable that deviations will occur if we move further away from the $\Delta(1232)$ peak. The $P_{11}(1440)$ resonance is the nearest nucleon resonance. Due to its large decay width, it is the most likely candidate to contribute to pion photoproduction on the high-energy tail of the $\Delta(1232)$. Since the $P_{11}(1440)$ contributes to the $M^{(1/2)}_{1-}$ multipole, we indeed find deviations for this multipole between our calculation and the data if we approach the $P_{11}(1440)$ energy region.

As has been outlined in Ref. [16], we describe the nonresonant transition operator $v^B_{\gamma\pi}$ by the tree diagrams of Fig. 2(b–e), as prescribed by an effective Lagrangian. The electromagnetic γNN and $\gamma\pi\pi$ vertices are well known as

$$\mathcal{L}_{\gamma NN} = -e\,\bar{\psi}_N\left[\hat{e}_N \gamma_\mu A^\mu - \frac{\kappa_N}{2M_N}\,\sigma_{\mu\nu}\,\partial^\nu A^\mu\right]\psi_N,$$
$$\mathcal{L}_{\gamma\pi\pi} = e[(\partial_\mu \boldsymbol{\pi})^\dagger \times \boldsymbol{\pi}]_3 A^\mu, \tag{12}$$

where A^μ is the electromagnetic vector potential, and ψ_N and $\boldsymbol{\pi}$ are the nucleon and pion field operators, respectively. Furthermore, κ_N is the nucleon anomalous magnetic moment ($\kappa_p = 1.79, \kappa_n = -1.91$).

In the low-energy regime addressed in this work, we use the πNN interaction Lagrangian with pseudovector coupling (PV),

$$\mathcal{L}^{PV}_{\pi NN} = \frac{f_{\pi NN}}{m_\pi}\,\bar\psi_N\,\gamma_\mu\gamma_5\,\boldsymbol{\tau}\,\psi_N\cdot\partial^\mu\boldsymbol{\pi}, \tag{13}$$

which is consistent with the leading order of chiral perturbation theory. In Eq. (13), $\boldsymbol{\tau}$ are the Pauli (isospin) matrices, and the coupling constant is taken as $f^2_{\pi NN}/4\pi = 0.081$. At higher energies, an improvement of the nonresonant multipoles can be obtained by a mixed pseudoscalar (PS)-pseudovector (PV) πNN coupling as, e.g., in the MAID analysis [16]. In the $\Delta(1232)$-resonance region considered in this work, we prefer to stay consistent with the leading order chiral perturbation theory and will use the PV coupling in the description of both the $\gamma p \to \pi N$ and $\gamma p \to \gamma\pi N$ reaction.

The relevant effective Lagrangians for the vector meson (ρ and ω) exchanges are shown in Fig. 2(b) and given by

$$\mathcal{L}_{V\pi\gamma} = \frac{e g_{V\pi\gamma}}{m_\pi}\,\varepsilon_{\mu\nu\rho\sigma}\,(\partial^\mu A^\nu)\,\pi_i\,\partial^\rho(\omega^\sigma\delta_{i3}+\rho_i^\sigma),$$

$$\mathcal{L}_{VNN} = g_{VNN}\bar\psi_N\left(\gamma_\mu V^\mu - \frac{\kappa_V}{2M_N}\sigma_{\mu\nu}\partial^\nu V^\mu\right)\psi_N, \tag{14}$$

where V denotes the ρ and ω vector meson fields. The photon couplings $g_{\rho\pi\gamma}$ and $g_{\omega\pi\gamma}$ can be obtained from the radiative decays $\rho\to\gamma\pi$ and $\omega\to\gamma\pi$, which lead to the values $g_{\rho^+\pi\gamma} = 0.103$, $g_{\rho^0\pi\gamma} = 0.131$, and $g_{\omega\pi\gamma} = 0.314$. For the hadronic couplings g_{VNN} and κ_{VNN}, we use the values $g_{\rho NN} = 2.63$, $\kappa_\rho = 6.1$, $g_\omega = 20$, and $\kappa_\omega = 0$. With these effective Lagrangians, it is straightforward to derive the amplitude shown in Fig. 2(b).

To calculate the $\Delta(1232)$ resonance contribution to $v^\Delta_{\gamma\pi}$ of Fig. 2(a), we use a form of the Rarita-Schwinger propagator [22],

$$\begin{aligned}\tilde G_{\alpha\beta}(p_\Delta) = \frac{\not p_\Delta + M_\Delta}{p^2_\Delta - M^2_\Delta}\Bigg\{ &-g_{\alpha\beta} + \frac{1}{3}\gamma_\alpha\gamma_\beta + \frac{1}{3M_\Delta}(\gamma_\alpha(p_\Delta)_\beta \\ &- \gamma_\beta(p_\Delta)_\alpha) + \frac{2}{3M^2_\Delta}(p_\Delta)_\alpha\,(p_\Delta)_\beta\Bigg\} - \frac{2}{3M^2_\Delta} \\ &\times\{\gamma_\alpha(p_\Delta)_\beta + \gamma_\beta(p_\Delta)_\alpha - \gamma_\alpha\,(\not p_\Delta - M_\Delta)\,\gamma_\beta\},\end{aligned} \tag{15}$$

where p_Δ is the four-momentum, and M_Δ is the mass of the $\Delta(1232)$. The interaction Lagrangians for the vertices $\pi N\Delta$ and $\gamma N\Delta$ are

$$\mathcal{L}_{\pi N\Delta} = \frac{f_{\pi N\Delta}}{m_\pi}\,\bar\psi^\mu_\Delta\,\boldsymbol{T}^\dagger\,\psi_N\cdot\partial_\mu\boldsymbol{\pi} + \text{h.c.}, \tag{16}$$

$$\mathcal{L}_{\gamma N\Delta} = i\,e\,\bar\psi^\mu_\Delta\,T^\dagger_3\,\Gamma_{\mu\nu}\,\psi_N\,A^\nu + \text{h.c.}, \tag{17}$$

where ψ^μ_Δ is the Rarita-Schwinger Δ field operator, and $\boldsymbol{T}$ is the $N\leftrightarrow\Delta$ isospin transition operator. The $\pi N\Delta$ coupling constant $f_{\pi N\Delta}$ in Eq. (16) is taken from the decay $\Delta\to\pi N$, which yields $f_{\pi N\Delta}\approx 1.95$. In Eq. (17), the $\gamma N\Delta$ coupling $\Gamma_{\mu\nu}$ has the form

$$\Gamma^{\mu\nu} = G_M\,\Gamma^{\mu\nu}_M + G_E\,\Gamma^{\mu\nu}_E, \tag{18}$$

where $\Gamma^{\mu\nu}_M$ and $\Gamma^{\mu\nu}_E$ denote the magnetic and electric $\gamma N\Delta$ vertices, respectively,

$$\Gamma^{\mu\nu}_M = -\frac{3}{4M_N}\,\frac{1}{(M_\Delta+M_N)}\,\varepsilon^{\mu\nu\kappa\lambda}(p_\Delta+p)_\kappa\,k_\lambda, \tag{19}$$

$$\begin{aligned}\Gamma^{\mu\nu}_E = -\Gamma^{\mu\nu}_M - \frac{3i\gamma_5}{(M_\Delta+M_N)(M_\Delta-M_N)^2\,M_N} \\ \times(\varepsilon^{\mu\sigma\kappa}(p_\Delta+p)_\kappa\,k_\lambda)\left(\varepsilon^\nu{}_\sigma{}^{\rho\tau}(p_\Delta)_\rho k_\tau\right).\end{aligned} \tag{20}$$

The magnetic and electric $\gamma N\Delta$ couplings G_M and G_E at the real photon point will be adjusted in the following.

Using the effective Lagrangians of Eqs. (16) and (17), we can write the Δ resonance contribution of Fig. 2(a) as

$$\begin{aligned}v^\Delta_{\gamma\pi} = -e\,C_{\pi N}\,\frac{f_{\pi N\Delta}}{m_\pi}\,q^\alpha\varepsilon_\mu(k,\lambda)\,\bar u(p',s'_N)\,\tilde G_{\alpha\beta}(p_\Delta) \\ \times\left[G_M\,\Gamma^{\beta\mu}_M + G_E\,\Gamma^{\beta\mu}_E\right]u(p,s_N),\end{aligned} \tag{21}$$

where $C_{\pi N} = 2/3$ for $\gamma p\to\pi^0 p$ and $-\sqrt{2}/3$ for $\gamma p\to\pi^+ n$, and $\tilde G_{\alpha\beta}$ is the Δ propagator given by Eq. (15).

To take account of the finite width of the $\Delta(1232)$ resonance, we follow the procedure of Refs. [14,22,29] by using a complex pole description for the resonance excitation. This amounts to the replacement

$$M_\Delta \longrightarrow M_\Delta - \frac{i}{2}\,\Gamma_\Delta, \tag{22}$$

in the propagator of Eq. (15). This "complex mass scheme" guarantees electromagnetic gauge invariance. In contrast, the use of a Breit-Wigner propagator with an energy dependent width will violate gauge invariance when applied to the Δ contribution for the $\gamma p\to\gamma\pi N$ reaction. For mass and width we take the complex pole values given by the PDG [8]: $(M_\Delta,\Gamma_\Delta) = (1210,100)$ MeV, which provides a good description of the photoproduction data.

Since our main goal is to explore the role of the $\Delta^+(1232)$ MDM in the $\gamma p\to\gamma\pi N$ reaction, it is not our purpose to precisely reproduce the pion photoproduction data over a large energy range. For example, the inclusion of an energy-dependence for the PS-PV mixing parameter and the use of a Breit-Wigner distribution with an energy dependent Δ decay width instead of the energy independent complex pole description can improve the description of the pion photoproduction data. However, these improvements would create problems in maintaining gauge invariance in the $\gamma p\to\gamma\pi N$ reaction, as discussed in detail in Sec. IV. Rather, our strategy is to determine the very small set of parameters within the model outlined above, which gives a reasonable description of the pion photoproduction in the $\Delta(1232)$ region, and then apply the same model to the $\gamma p\to\gamma\pi N$ reaction.

In Fig. 3, we show our results for the total $\gamma p\to\pi^0 p$ cross section with the parameters $G_M = 3.00$ and $G_E = 0.065$, and compare them with the data from Refs. [23–26]. The solid curve denotes the results obtained with our full unitary model, and the dotted curve indicates the unitarized Δ resonance contributions of Eq. (11). If we approximate the t-matrix by the transition potential of Eq. (5) and replace $M_\Delta\to M_\Delta - \frac{i}{2}\Gamma_\Delta$, we obtain the tree-level result represented by the dashed curve. This corresponds to the previous results of Ref. [14],

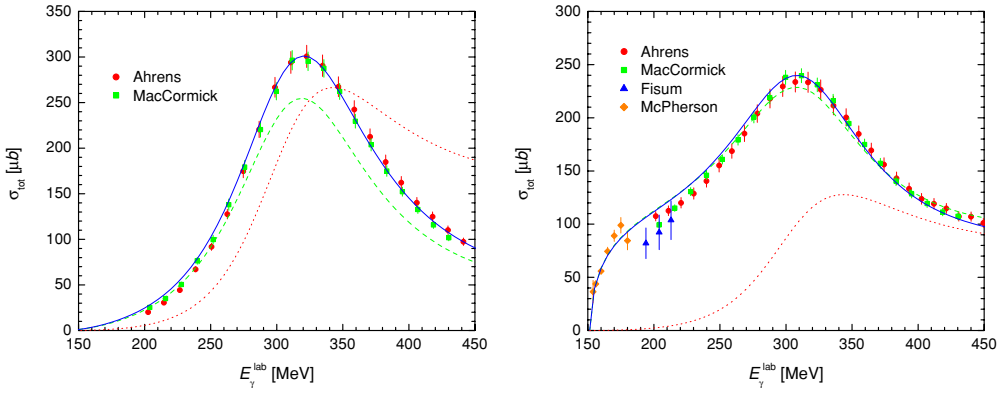

FIG. 3. (Color online) Total cross section for $\gamma p \to \pi^0 p$ (left panel) and $\gamma p \to \pi^+ n$ (right panel). The solid curve is the full result of the unitary model; the dashed curve indicates the result of the tree-level calculation; and the dotted curve shows the unitarized $\Delta(1232)$ contribution. The data for $\gamma p \to \pi^0 p$ are from MacCormick [23] and Ahrens [24]. The data for $\gamma p \to \pi^+ n$ are from MacCormick [23], Ahrens [24], McPherson [25], and Fissum [26].

except that we use the above values of G_M and G_E. We find that the fully unitary model describes the total cross sections for both the $\gamma p \to \pi^0 p$ and $\gamma p \to \pi^+ n$ reactions very well from threshold to $E_\gamma^{\rm lab} = 450$ MeV, as is shown in Fig. 3. The difference between the unitarized result and the tree-level calculation indicates the size of the rescattering effects, which turns out to be relatively large for the $\gamma p \to \pi^0 p$ reaction. We find that even though one can improve the description of the total cross sections within the tree-level approximation by adjusting the model parameters G_M and G_E, it is not possible to achieve a satisfactory tree-level description for the differential and polarization cross sections discussed next.

The results for the differential cross sections for $\gamma p \to \pi^0 p$ are shown in Fig. 4 (left panel). They agree well with the data from Refs. [27,28] except for the highest energy

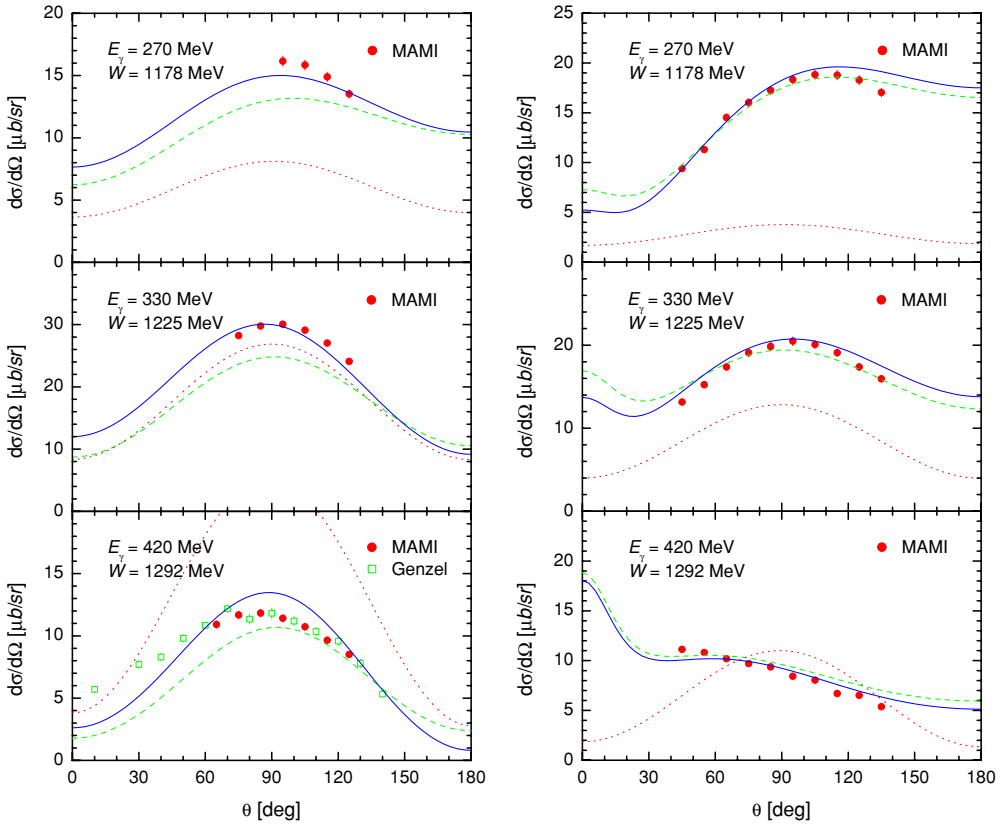

FIG. 4. (Color online) Differential cross section for the $\gamma p \to \pi^0 p$ reaction (left panel) and $\gamma p \to \pi^+ n$ reaction (right panel) at different photon *lab* energies E_γ as a function of the c.m. angle θ. The data are from Bonn [27] and MAMI [28]. See Fig. 3 for further notation.

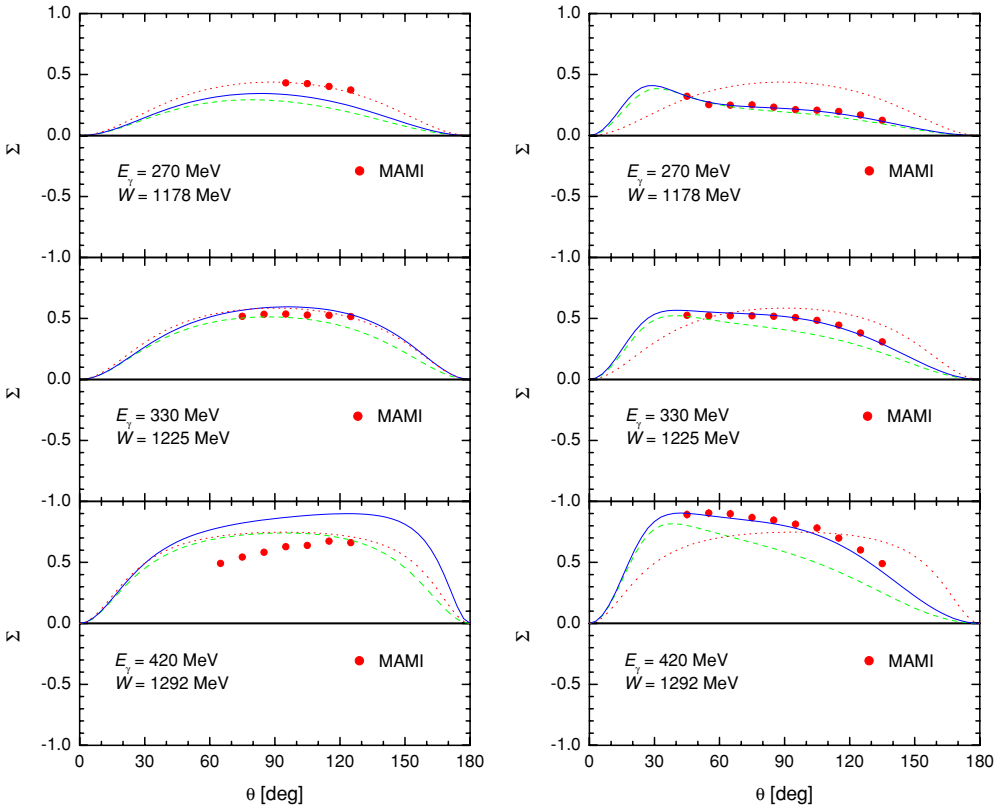

FIG. 5. (Color online) Beam asymmetry for $\gamma p \to \pi^0 p$ (left panel) and $\gamma p \to \pi^+ n$ (right panel) at different photon *lab* energies E_γ as a function of the c.m. angle θ. The data are from MAMI [28]. See Fig. 3 for further notation.

$E_\gamma^{\rm lab} = 420$ MeV. The deviation may be traced back to the fact that the Δ propagator of Eq. (15) contains an additional spin-1/2 component. In the case of charged pion photoproduction, the angular distribution shows an interference pattern between background and resonance contributions, which leads to an enhancement of backward production below the resonance and a sharp rise in the forward direction above the resonance.

The beam asymmetries for neutral and charged pion production are shown in Fig. 5. While we observe some deviations between the model and the neutral pion data at the highest energy, the process $\gamma p \to \pi^+ n$ is well described over the full energy range. In particular we note a considerable improvement of the angular distribution due to the unitarization effects.

Recently, the helicity dependent total cross sections $\sigma_{3/2}$ ($\sigma_{1/2}$) for the absorption of circularly polarized photons on nucleons in total helicity states of 3/2 (1/2) have been measured for the $\gamma p \to \pi^0 p$ and $\gamma p \to \pi^+ n$ reactions [24]. We show the comparison between our unitary model and these data in Fig. 6. For the $\gamma p \to \pi^0 p$ reaction the $\sigma_{3/2}$ cross section is dominated by the $\Delta(1232)$ resonance, which yields positive values of $\sigma_{3/2} - \sigma_{1/2}$ over the full energy region. For the $\gamma p \to \pi^+ n$ channel, however, the strong nonresonant pion production leads to a large $\sigma_{1/2}$ cross section near threshold followed by $\sigma_{3/2}$ dominance in the $\Delta(1232)$ region. Altogether we obtain a qualitatively good description of the helicity dependent cross sections for both $\gamma p \to \pi^0 p$ and $\gamma p \to \pi^+ n$, with some deviations appearing on the high-energy side of the $\Delta(1232)$ region.

Figure 7 shows the multipole amplitudes in the Δ channel, M_{1+} and E_{1+}, obtained with our best fit values $G_M = 3.0$ and $G_E = 0.065$. These results are compared with the SM02 solution of the SAID partial wave analysis [30]. The unitarized model reproduces the dominant $M_{1+}^{(3/2)}$ multipoles from SAID quite well, whereas the agreement is less perfect for the $E_{1+}^{(3/2)}$ multipole. However, since the latter multipole is small ($G_E/G_M \sim 2\%$), these deviations are of little importance for our conclusions. As stated above, the inclusion of higher resonances such as the $P_{11}(1440)$ could improve our calculation at the larger energies. However, a consistent description of these higher resonances is outside the scope of our current study and we therefore leave it for a future work.

IV. UNITARY MODEL FOR THE $\gamma p \to \gamma \pi N$ REACTION

In this section we extend the previously constructed model for pion photoproduction to the reaction $\gamma p \to \gamma \pi N$ in the $\Delta(1232)$-resonance region, which will then be used as a tool to investigate the size of the $\Delta(1232)$ MDM. After discussing the tree-level processes for the $\gamma p \to \gamma \pi N$ reaction, we subsequently extend this description and present a unitary model for the $\gamma p \to \gamma \pi^0 p$ reaction in the $\Delta(1232)$ region.

We start from the tree diagrams in Fig. 2 as prescribed by the effective Lagrangian for $\gamma p \to \pi N$ and couple a

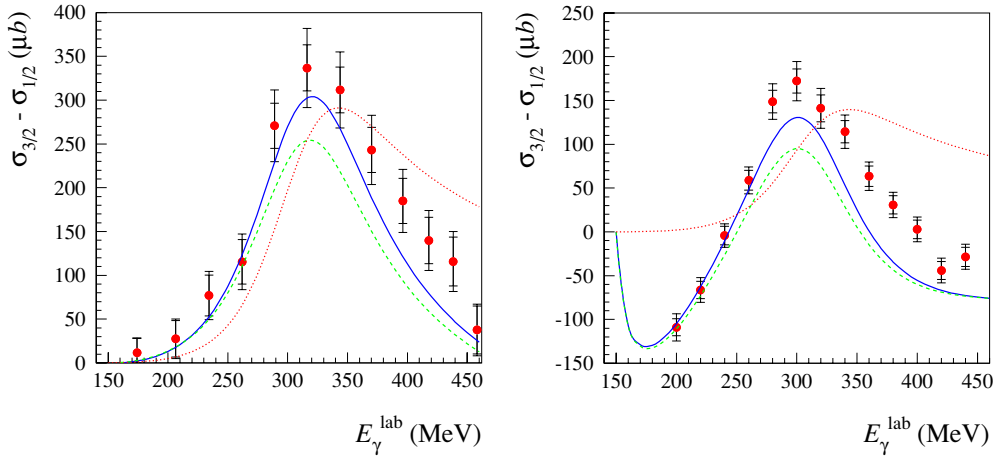

FIG. 6. (Color online) Helicity cross-section difference $\sigma_{3/2} - \sigma_{1/2}$ for the $\gamma p \to \pi^0 p$ reaction (left panel) and the $\gamma p \to \pi^+ n$ reaction (right panel). The data are from MAMI [24]: inner error bars correspond with statistical errors; outer error bars include systematical errors. See Fig. 3 for further notation.

photon to all the charged particles. The resulting diagrams are shown in in Fig. 8. The diagrams in Fig. 8(b–e) referring to vector-meson exchanges, nucleon and pion pole, as well as Kroll-Ruderman terms can be evaluated with the interaction Lagrangians given in Sec. III or by minimal substitution of pion-nucleon Lagrangians given in that section. For example, the $\gamma\pi NN$ and $\gamma\gamma\pi\pi$ vertices can be obtained by replacing the derivative ∂^μ in $\mathcal{L}_{\pi NN}$ and $\mathcal{L}_{\gamma\pi\pi}$ by the covariant derivative $\partial^\mu + iQA^\mu$, where Q is the charge of the respective pion. By design, this set of diagrams is therefore gauge invariant by itself with respect to both initial and final photons. In Fig. 8, we display the diagrams for both the $\gamma p \to \gamma \pi^0 p$ and the $\gamma p \to \gamma \pi^+ n$ reaction. When omitting the coupling to the pion lines and the contact diagrams, diagrams (a–c) yield the tree diagrams considered in Ref. [14]. In addition to Ref. [14], we include the diagrams in Fig. 8(f) resulting from the $\pi^0 \to \gamma\gamma$ anomaly as given by the Wess-Zumino-Witten Lagrangian [31],

$$L_{WZW} = \frac{\alpha_{em}}{8\pi F_\pi} \epsilon_{\mu\nu\alpha\beta} F^{\mu\nu} F^{\alpha\beta} \pi^0, \tag{23}$$

with $F^{\mu\nu} = \partial^\mu A^\nu - \partial^\nu A^\mu$, and $F_\pi = 92.4$ MeV the pion decay constant. Note that in the soft photon limit for the final photon, i.e., $k' \to 0$, the anomaly diagrams vanish as they are linear in the final photon momentum k'.

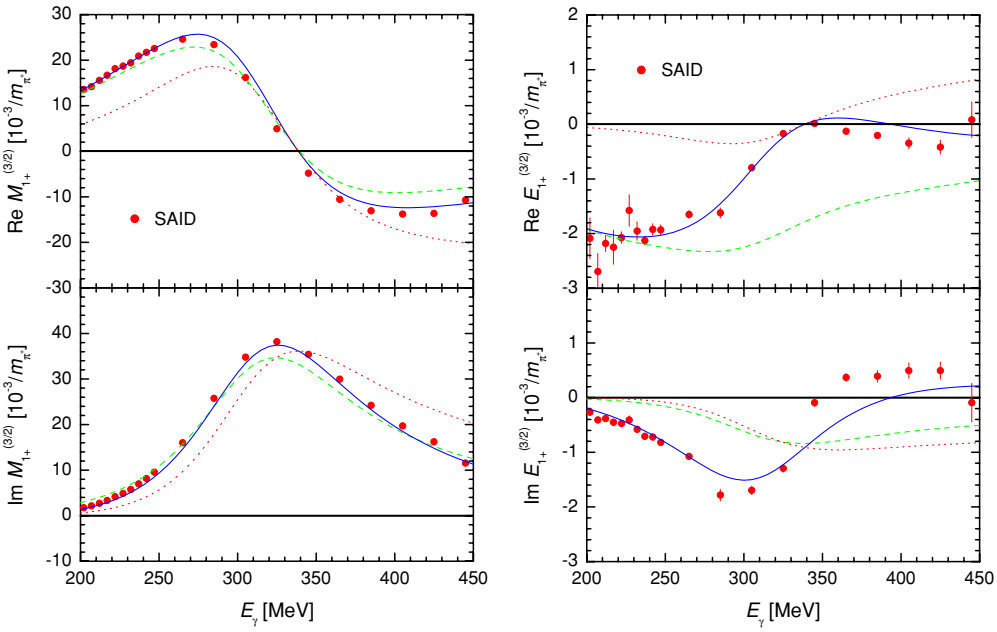

FIG. 7. (Color online) Multipole amplitudes $M_{1+}^{(3/2)}$ (left panel) and $E_{1+}^{(3/2)}$ (right panel) for pion photoproduction as a function of the photon *lab* energy E_γ. The data are taken from the SAID analysis [30]. See Fig. 3 for further notation.

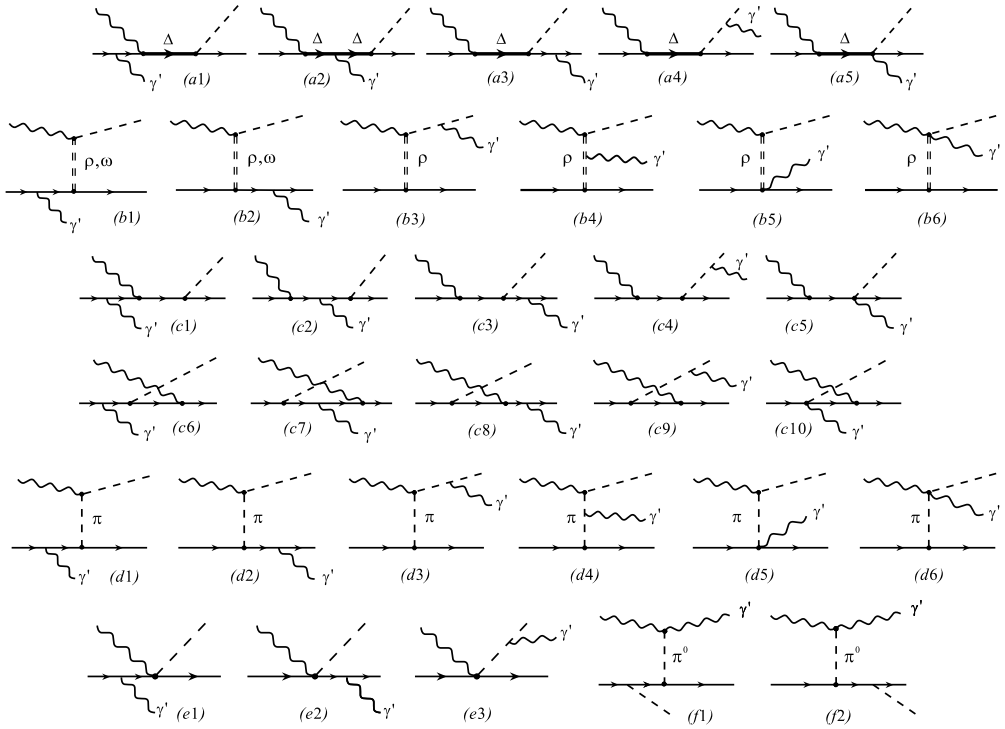

FIG. 8. Tree diagrams considered in the calculation of the $\gamma p \to \gamma \pi N$ reaction in the $\Delta(1232)$ region: Δ resonance (a1–a5), vector-meson exchange (b1–b6), nucleon-pole (c1–c10), pion-pole (d1–d6), Kroll-Rudermann (e1–e3), and anomaly (f1–f2) diagrams.

The Δ resonance diagrams of Fig. 8(a) can be similarly evaluated by use of the previously described Lagrangians except for diagram 8(a2). The latter diagram contains the interaction Lagrangian

$$L_{\gamma\Delta\Delta} = e_\Delta \bar{\psi}^{\beta'}_\Delta \left\{ g_{\beta'\beta} \left(\gamma_\nu A^\nu - \frac{\kappa_\Delta}{2M_\Delta} \sigma_{\nu\lambda}\, \partial^\lambda A^\nu \right) + \frac{1}{3} (\gamma_\beta \gamma_\nu \gamma_{\beta'} - \gamma_\beta g_{\nu\beta'} - \gamma_{\beta'} g_{\nu\beta}) A^\nu \right\} \psi^\beta_\Delta, \quad (24)$$

which contains the information on κ_Δ, the anomalous magnetic moment (a.m.m.) of the $\Delta(1232)$ resonance.

The magnetic moment μ of a particle of mass M, charge e, and spin S can in general be expressed in terms of the gyromagnetic ratio g as

$$\mu = g \cdot S \cdot \frac{e}{2M}. \quad (25)$$

It was argued in Refs. [32,33] that $g = 2$ corresponds with the the universal value for the gyromagnetic ratio for a point particle with arbitrary spin. The minimal electromagnetic coupling in Eq. (24) corresponds with $g = 1/S$ [where $S = 3/2$ in Eq. (24)]. The deviation from this value corresponds with the term in Eq. (24) proportional to κ_Δ, defined as

$$\kappa_\Delta = g_\Delta \cdot \frac{3}{2} - 1. \quad (26)$$

Note that with this definition the value $g_\Delta = 2$ corresponds with $\kappa_\Delta = 2$.

In comparison with the $\gamma p \to \pi N$ process, the only new parameter entering into the description of the $\gamma p \to \gamma \pi N$ process is the $\Delta^+(1232)$ anomalous magnetic moment κ_{Δ^+}. The $\gamma\Delta\Delta$ vertex of Eq. (24) satisfies the electromagnetic Ward identity with the Δ propagator of Eq. (15). Gauge invariance is preserved when using the complex pole description of Eq. (22).

In principle, the $\gamma\Delta\Delta$ vertex and hence κ_Δ is a function of k'^2, p^2_Δ, p'^2_Δ, the four-momentum squared of the emitted photon, and the initial and final Δ, respectively. As we are studying the transition induced by real photons, $k'^2 = 0$. If we restrict ourself to the $\Delta(1232)$-resonance region, then we can choose $p^2_\Delta = M^2_\Delta$, and κ_Δ will depend only on p'^2_Δ. In the soft-photon limit, we will further have $p'^2_\Delta = M^2_\Delta$. By assuming that κ_Δ is a slowly varying function of p'^2_Δ, we can then treat κ_Δ as a constant in the soft-photon region. We confines ourselves to this kinematical region in our current investigation.

We next turn to the rescattering contribution for the $\gamma p \to \gamma \pi^0 p$ reaction. In this work, we estimate this rescattering in the K-matrix approximation, i.e., considering only onshell rescattering. Furthermore, in the soft-photon limit for the final photon, the T matrix for the $\gamma p \to \gamma \pi^0 p$ reaction has to be directly proportional to the full T matrix for the $\gamma p \to \pi^0 p$ reaction as previously constructed (see Fig. 1). We construct the full T matrix for $\gamma p \to \gamma \pi^0 p$ as shown in Fig. 9 by the expression

$$t_{\gamma,\gamma\pi}(\boldsymbol{k'q}, W_{\pi N}; \boldsymbol{k}, \sqrt{s}) \approx v_{\gamma,\gamma\pi}(\boldsymbol{k'q}; \boldsymbol{k}) + e\, \varepsilon^*_\nu(k', \lambda') \times \left(\frac{p'^\nu}{p' \cdot k'} - \frac{p^\nu}{p \cdot k'} \right) [t_{\gamma\pi}(\boldsymbol{q}, \boldsymbol{k}; \sqrt{s}) - v_{\gamma\pi}(\boldsymbol{q}, \boldsymbol{k})]. \quad (27)$$

The first term in Eq. (27), denoted by the transition potential $v_{\gamma,\gamma\pi}$, is the sum of all tree diagrams shown in Fig. 8. As discussed above, this term is gauge invariant by itself with

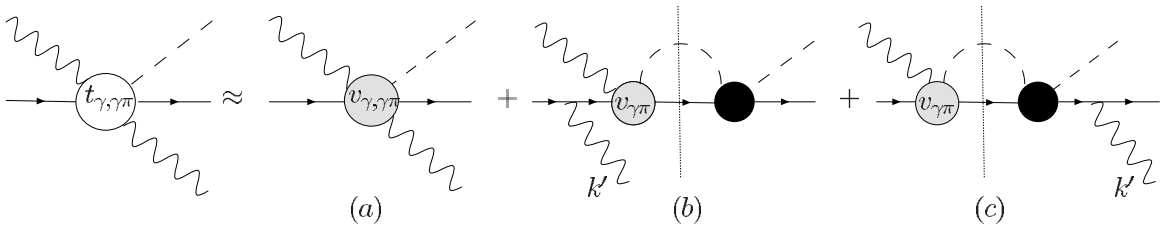

FIG. 9. Model for the T matrix for the $\gamma p \to \gamma \pi^0 p$ reaction used in this work. The transition potential $v_{\gamma,\gamma\pi}$ (diagram a) corresponds with the diagrams of Fig. 8. The rescattering contributions (diagrams b and c) are evaluated in the soft-photon approximation for the final photon, i.e., $k' \to 0$. The transition potential $v_{\gamma\pi}$ corresponds with the diagrams of Fig. 2. The black circle corresponds with the full T-matrix $t_{\pi N}$ for πN scattering. The vertical dotted lines indicate that the πN intermediate state is taken onshell (K-matrix approximation).

respect to both intial and final photons. In the soft-photon limit (i.e., $k' \to 0$), it reduces to

$$v_{\gamma,\gamma\pi}(\boldsymbol{k'q};\boldsymbol{k}) \overset{k'\to 0}{\longrightarrow} e\,\varepsilon_\nu^*(k',\lambda')\left(\frac{p'^\nu}{p'\cdot k'} - \frac{p^\nu}{p\cdot k'}\right) v_{\gamma\pi}(\boldsymbol{q},\boldsymbol{k}), \tag{28}$$

where $v_{\gamma\pi}$ is the transition potential for the $\gamma p \to \pi^0 p$ reaction as shown in Fig. 2. The second term in Eq. (27) is the rescattering contribution. Since we only keep the leading term in the outgoing photon energy for the rescattering term ($k' \to 0$), this amounts to evaluating the T-matrix $t_{\gamma\pi}$ in the second term of Eq. (27) in soft-photon kinematics, i.e., with nucleon momenta $\boldsymbol{p} = -\boldsymbol{k}$, $\boldsymbol{p'} = -\boldsymbol{q}$, and at total energy $\sqrt{s}$, with $s = (k+p)^2$, as we work in the c.m. system of the $\gamma p \to \gamma\pi N$ reaction. For the t-matrix $t_{\gamma\pi}$, we adopt the unitary model as discussed in Sec. III. Evaluating the rescattering term for the $\gamma p \to \gamma\pi N$ process in the soft-photon limit, as done in Eq. (27), ensures us that the full amplitude $t_{\gamma,\gamma\pi}$ satisfies the low-energy theorem. Indeed, using Eq. (28), we immediately verify from Eq. (27) that

$$t_{\gamma,\gamma\pi}(\boldsymbol{k'q}, W_{\pi N};\boldsymbol{k},\sqrt{s}) \overset{k'\to 0}{\longrightarrow} e\,\varepsilon_\nu^*(k',\lambda') \times \left(\frac{p'^\nu}{p'\cdot k'} - \frac{p^\nu}{p\cdot k'}\right) t_{\gamma\pi}(\boldsymbol{q},\boldsymbol{k};\sqrt{s}), \tag{29}$$

as required by the low-energy theorem.

Furthermore, both terms in our model for the full T-matrix $t_{\gamma,\gamma\pi}$ in Eq. (27) satisfy gauge invariance with respect to both intial and final photons. One notices in particular that the rescattering contribution [the second term in Eq. (27)] is by construction gauge invariant with respect to the final photon [as is evident when replacing $\varepsilon^*(k',\lambda')$ by k']. We further point out that the rescattering contributions of Fig. 9(b) and (c) are obtained by summing over both $\pi^+ n$ and $\pi^0 p$ intermediate states in the loop.

To evaluate the rescattering contribution beyond the soft-photon limit is much more complicated and requires a coupled channel calculation for both the $\gamma N \to \gamma\pi N$ and $\pi N \to \gamma\pi N$ processes, because the outgoing photon can be produced not only in the initial step but also by a pion while rescattering off the nucleon. Furthermore, the exact conservation of gauge invariance in such an approach requires the introduction of vertex corrections wherever the photon is emitted between two different pion rescatterings. We leave such a description for a future work, because our evaluation of the rescattering effects for the $\gamma p \to \gamma\pi^0 p$ process is motivated by the experimental situation where one stays relatively close to the soft-photon limit, i.e., at outgoing photon energies up to about 100 MeV. Furthermore, for the tree-level contribution $v_{\gamma,\gamma\pi}$ in Eq. (27), we do not make a soft-photon approximation but calculate the full outgoing photon energy dependence. Because the effect of the rescattering turns out to be modest in all the following calculations, it is a reasonable approximation to evaluate the rescattering contribution in the soft-photon limit for those kinematics.

V. RESULTS AND DISCUSSION FOR $\gamma p \to \gamma\pi N$ OBSERVABLES

In Fig. 10, we show the outgoing photon energy dependence of the cross-section $d\sigma/dE'_\gamma$ for the $\gamma p \to \gamma\pi^0 p$ reaction integrated over the photon and pion angles for three incoming photon energies through the $\Delta(1232)$ region. Because the cross sections exhibit the characteristic bremsstrahlung behavior, i.e., dropping as $1/E'_\gamma$ at low energies E'_γ, we display the cross sections in the left panel of Fig. 10 multiplied by E'_γ.

In the soft-photon limit ($E'_\gamma \to 0$), gauge invariance provides a model-independent relation between the cross sections for the $\gamma p \to \gamma\pi N$ and $\gamma p \to \pi N$ reactions. This low-energy theorem was derived in Ref. [34] for radiative photoproduction of a neutral meson. In the Appendix, we first apply this theorem to the $\gamma p \to \gamma\pi^0 p$ reaction and then extend it to the $\gamma p \to \gamma\pi^+ n$ process. Its derivation is based on the observation that in the soft-photon limit the $\gamma p \to \gamma\pi N$ reaction is completely determined by the bremsstrahlung process from the initial and final protons. In this limit, when integrating the fivefold differential cross section of Eq. (1) over the outgoing photon angles, we obtain the threefold differential cross section for the $\gamma p \to \gamma\pi N$ process, which reduces in the soft-photon limit to

$$\left(\frac{d\sigma}{dE'_\gamma\, d\Omega_\pi}\right)^{\text{c.m.}} \overset{E'_\gamma\to 0}{\longrightarrow} \frac{1}{E'_\gamma}\cdot\frac{e^2}{2\pi^2}\cdot W(v)\left(\frac{d\sigma}{d\Omega_\pi}\right)^{\text{c.m.}}, \tag{30}$$

where $(d\sigma/d\Omega_\pi)^{\text{c.m.}}$ is the differential cross section for the $\gamma p \to \pi N$ process. The form of the angular weight-function $W(v)$ is derived in the Appendix, Sec. A, as

$$W(v) = -1 + \left(\frac{v^2+1}{2v}\right)\cdot \ln\left(\frac{v+1}{v-1}\right), \tag{31}$$

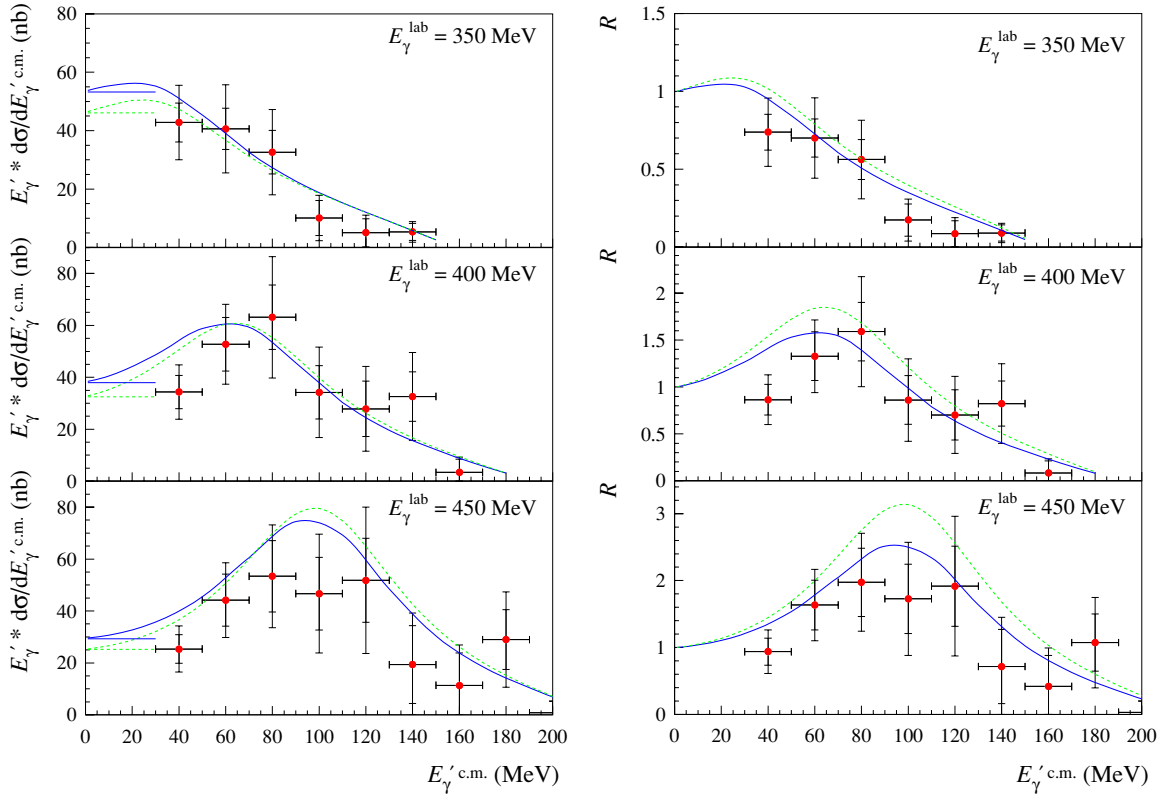

FIG. 10. (Color online) Left panel: outgoing photon energy dependence of the cross-section $d\sigma/dE_\gamma'^{\rm c.m.}$ multiplied by $E_\gamma'^{\rm c.m.}$ for the $\gamma p \to \gamma\pi^0 p$ reaction. A comparison is shown between the tree-level calculation (dashed curves) and the result of the unitary model (solid curves). All results are obtained with $\kappa_{\Delta^+} = 3$. The horizontal curves at small values of $E_\gamma'^{\rm c.m.}$ are obtained using the low-energy theorem for the tree-level model (thin dashed curves) and the unitary model (thin solid curves). Right panel: ratio R, as defined in Eq. (34), for the $\gamma p \to \gamma\pi^0 p$ reaction and with the same conventions as in the left panel. The data in both panels are from MAMI [10]: inner error bars correspond to statistical errors; outer error bars include systematical errors.

with $v \equiv \sqrt{1 + 4M_N^2/(-t)}$ and $t = (p' - p)^2$. When integrating the fivefold differential cross section of Eq. (1) over both the outgoing photon and the meson angles, we obtain the energy distribution for the $\gamma p \to \gamma\pi N$ process as

$$\left(\frac{d\sigma}{dE'_\gamma}\right)^{\rm c.m.} \equiv \int d\Omega_\pi^{\rm c.m.} \left(\frac{d\sigma}{dE'_\gamma d\Omega_\pi}\right)^{\rm c.m.} \stackrel{E'_\gamma \to 0}{\longrightarrow} \frac{1}{E'_\gamma} \cdot \sigma_\pi , \tag{32}$$

with a "weight-averaged" total cross-section σ_π for the $\gamma p \to \pi N$ reaction,

$$\sigma_\pi \equiv \frac{e^2}{2\pi^2} \int d\Omega_\pi^{\rm c.m.}\, W(v) \left(\frac{d\sigma}{d\Omega_\pi}\right)^{\rm c.m.} . \tag{33}$$

The low-energy theorem of Eq. (32) provides a check for both theoretical model calculations and experimental measurements, because

$$R \equiv \frac{1}{\sigma_\pi} \cdot E'_\gamma \frac{d\sigma}{dE'_\gamma} \to 1 \quad \text{for } E'_\gamma \to 0. \tag{34}$$

At small values of E'_γ, one readily observes from Fig. 10 (left panel) that our theoretical calculation for the product $E'_\gamma \cdot d\sigma/dE'_\gamma$ approaches a constant. Because we model the $\gamma p \to \pi^0 p$ and $\gamma p \to \gamma\pi^0 p$ reactions within the same framework, the low-energy theorem is exactly satisfied, as follows from Eq. (28) for the tree-level model and Eq. (29) for the unitary model. In the right panel of Fig. 10, we show the ratio R constructed from our theoretical calculations of the $\gamma p \to \gamma\pi^0 p$ and $\gamma p \to \pi^0 p$ reactions and compare it with the data of Ref. [10] for this same ratio, where σ_π is evaluated from the $\gamma p \to \pi^0 p$ data using Eq. (34). The first data for the $\gamma p \to \gamma\pi^0 p$ process of Ref. [10] show a clear deviation from the soft-photon limit value $R = 1$ with increasing values of E'_γ. One sees from Fig. 10 that our unitary model gives a good overall description of the E'_γ dependence of the $\gamma p \to \gamma\pi^0 p$ reaction throughout the Δ-region. Compared with the tree-level model developed in Ref. [14], our unitary model reduces the cross section at larger values of E'_γ and thus provides an improved description of the data.

In Fig. 11, we show the outgoing photon angular dependence of the c.m. cross section $d\sigma/d\Omega'_\gamma$ for the $\gamma p \to \gamma\pi^0 p$ reaction, which has also been measured in Ref. [10]. To compare with these data, the cross section is integrated over the pion angles and over the outgoing photon energy range $E_\gamma'^{\rm c.m.} > 30$ MeV. Our model reproduces the angular dependence of the existing data, within their accuracy range, rather well. We see that the model gives a rather flat angular distribution at $E_\gamma^{\rm lab} = 350$ MeV. At higher incident photon

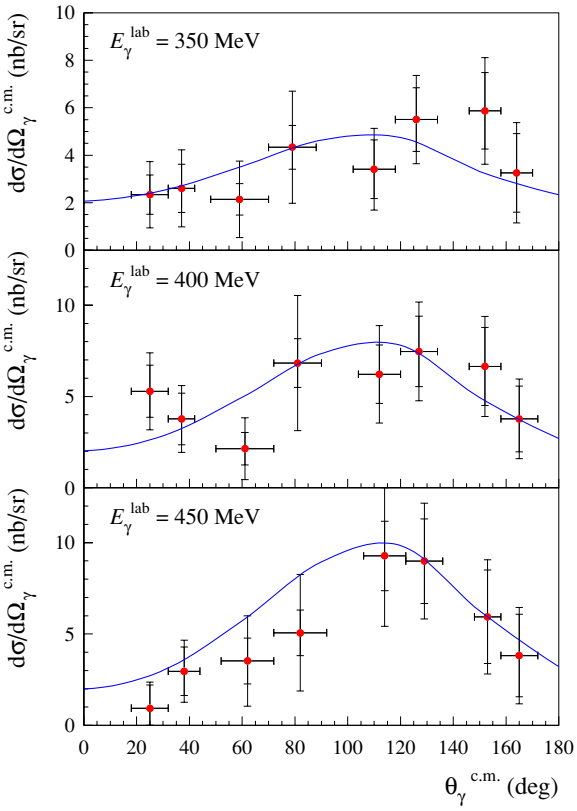

FIG. 11. (Color online) The angular distribution of the emitted photons for the $\gamma p \to \gamma \pi^0 p$ c.m. cross-section $d\sigma/d\Omega_\gamma^{c.m.}$. The cross section is integrated over the pion angles and over the outgoing photon energy range $E_\gamma'^{c.m.} > 30$ MeV. The results of the unitary model are shown with $\kappa_{\Delta^+} = 3$. The data are from MAMI [10]: inner error bars correspond tostatistical errors; outer error bars include systematical errors.

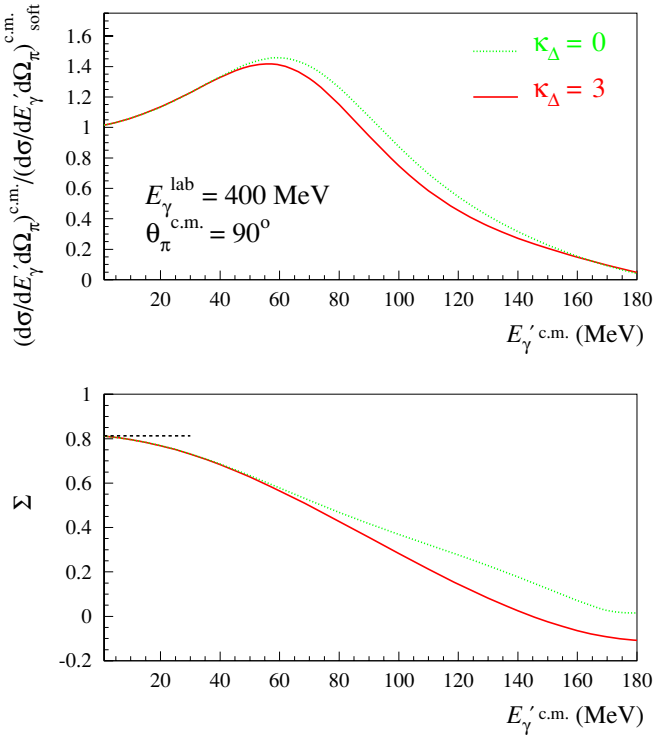

FIG. 12. (Color online) Top: the outgoing photon energy dependence of the $\gamma p \to \gamma \pi^0 p$ threefold differential c.m. cross-section $d\sigma/dE_\gamma' d\Omega_\pi$, divided by its value in the soft-photon limit, as a function of the outgoing photon energy $E_\gamma'^{c.m.}$, at incident photon *lab* energy $E_\gamma^{lab} = 400$ MeV and pion emission angle $\theta_\pi^{c.m.} = 90°$. Predictions of the unitary model for $\kappa_{\Delta^+} = 0$ (dotted curve) and $\kappa_{\Delta^+} = 3$ (full curve). Bottom: same for the photon asymmetry Σ. The horizontally dashed curve at small values of $E_\gamma'^{c.m.}$ is obtained using the low-energy theorem and corresponds to the photon asymmetry for the $\gamma p \to \pi^0 p$ reaction.

energies, it displays a broad peak around photon c.m. angles of 110°. Such a structure is due to the interference between the bremsstrahlung and Δ-resonant mechanisms. Note that a pure Δ-resonant mechanism would yield a photon angular distribution peaked around a c.m. angle of 90°. Comparing the unitary model with the data presented in Figs. 10 and 11, we conclude that both the outgoing photon energy and angular distributions of the $\gamma p \to \gamma \pi^0 p$ reaction through the Δ-region show clear deviations from a pure bremsstrahlung-dominated process as obtained in the soft-photon limit.

We next study how to extract new resonance information from the deviations from the soft-photon limit in the $\gamma p \to \gamma \pi^0 p$ cross sections at the larger values of E_γ'. In Fig. 12 we show the sensitivity of the threefold differential cross sections and the photon asymmetry, for linearly polarized incident photons, to the $\Delta^+(1232)$ MDM. We present both cross section and photon asymmetry at an incident photon energy of 400 MeV, for which our model yields a good description of the $\gamma p \to \pi^0 p$ observables. This serves as a reliable baseline to study the dependence of the $\gamma p \to \gamma \pi^0 p$ process on κ_{Δ^+} at the larger values of E_γ'. It can be seen from Fig. 12 that an outgoing photon energy E_γ' of around 100 MeV is a good compromise to enhance the sensitivity to κ_{Δ^+} while still staying in the region of validity of the present calculation, which treats the radiation due to rescattering effects in the soft-photon approximation.

In Fig. 13 we therefore investigate the sensitivity of the pion angular distribution at $E_\gamma^{lab} = 400$ MeV and $E_\gamma'^{c.m.} = 100$ MeV with regard to the value of κ_{Δ^+}. The upper part of Fig. 13 shows a considerable change in the angular distribution of the differential cross section when varying κ_{Δ^+} between 0 and 6. However, it is also obvious that extracting a value of κ_{Δ^+} from a fit to the angular distribution would require very accurate data over the whole angular range. The reason is that the differential cross section first decreases when increasing κ_{Δ^+} from the value $\kappa_{\Delta^+} = 0$, then reaches a minimum around a value $\kappa_{\Delta^+} = 3$, and increases subsequently when increasing κ_{Δ^+} further. This behavior is due to interference and evidently complicates an accurate extraction of κ_{Δ^+} from the differential cross section. However, we found that the photon asymmetry, for linearly polarized incident photons, decreases monotonically when increasing κ_{Δ^+}, as is displayed in the lower part of Fig. 13. In particular, the photon asymmetry varies between +0.35 and −0.15 when varying κ_{Δ^+} from 0 to 6.

Besides the photon asymmetry, for linearly polarized incident photons, we have also studied the single asymmetry

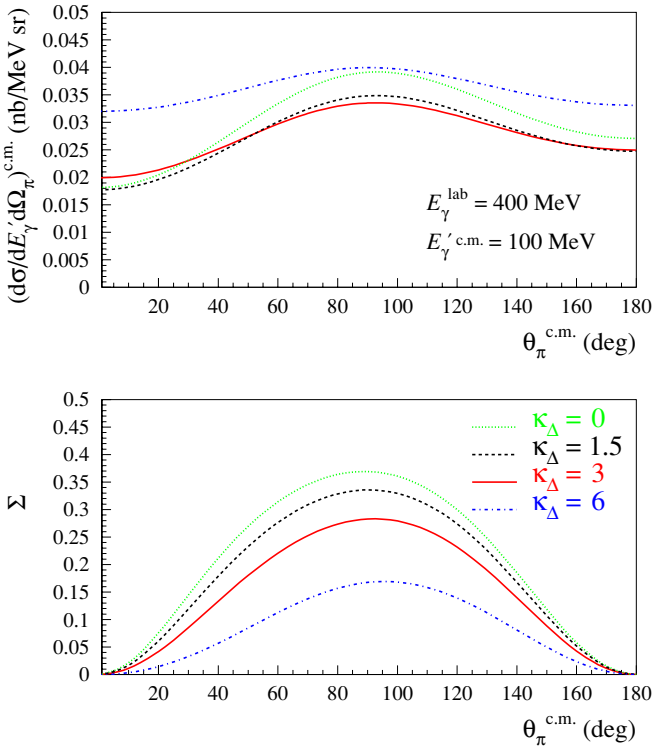

FIG. 13. (Color online) Top: the angular distribution of the emitted pions for the $\gamma p \to \gamma \pi^0 p$ threefold differential *c.m.* cross section $d\sigma/dE'_\gamma d\Omega_\pi$ at incident photon lab energy $E_\gamma^{lab} = 400$ MeV and fixed outgoing photon energy $E_\gamma'^{c.m.} = 100$ MeV. The sensitivity of the unitary model to different values of κ_{Δ^+} is shown. Bottom: same for the photon asymmetry Σ.

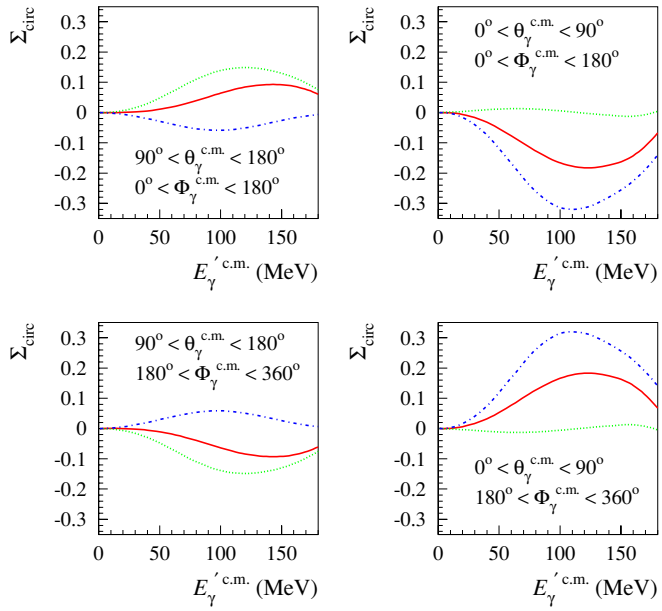

FIG. 14. (Color online) The outgoing photon energy dependence of the $\gamma p \to \gamma \pi^0 p$ single spin asymmetry Σ_{circ} for a circularly polarized incident photon at incident photon *lab* energy $E_\gamma^{lab} = 400$ MeV and pion emission angle $\theta_\pi^{c.m.} = 90^\circ$, when integrating over the outgoing photon angles as indicated on the figure. Predictions of the unitary model are shown for $\kappa_{\Delta^+} = 0$ (dotted curves), $\kappa_{\Delta^+} = 3$ (solid curves), and $\kappa_{\Delta^+} = 6$ (dashed-dotted curves).

for a circularly polarized incident photon, which we denote as Σ_{circ}. For a two-body reaction, such as $\gamma N \to \pi N$, parity conservation forces Σ_{circ} to vanish exactly because of the reflection symmetry with respect to the reaction plane. For a three-body process, such as $\gamma N \to \gamma \pi N$, this reflection symmetry is broken due to the emission of the second particle, and one can define a single spin asymmetry for circularly polarized photons as

$$\Sigma_{circ} \equiv \frac{d\sigma(\lambda = +1) - d\sigma(\lambda = -1)}{d\sigma(\lambda = +1) + d\sigma(\lambda = -1)}, \qquad (35)$$

where $d\sigma$ in Eq. (35) stands for $\left(d\sigma/dE'_\gamma d\Omega_\gamma d\Omega_\pi\right)^{c.m.}$, and $\lambda = \pm 1$ are the two circular polarization states of the incident photon. In Fig. 14, we show Σ_{circ} for the $\gamma p \to \gamma \pi^0 p$ reaction as a function of the outgoing photon energy when the pion is emitted at an angle $\theta_\pi^{c.m.} = 90^\circ$, which fixes the reaction plane. One may then study the dependence of Σ_{circ} when integrating $d\sigma$ over the angles of the outgoing photon. In Fig. 14, we separated the phase space for the outgoing photon into 4 quadrants, as the photon can be emitted in the forward or backward (with regard to the direction of the incident photon) hemispheres, and either above or below (with regard to the direction of $\vec{k} \times \vec{q}$) the reaction plane. One immediately observes from Fig. 14 that the sign of Σ_{circ} differs for photons emitted above and below the reaction plane. As a result, the integral of Σ_{circ} over the full solid angle of the final photon vanishes, because this way one effectively obtains the result of a two-body reaction. A further interesting feature of Fig. 14 is that Σ_{circ} vanishes exactly in the soft-photon limit. This can also be easily understood from the fact that in the soft-photon limit the LET relates the $\gamma N \to \gamma \pi N$ process to the two-body reaction $\gamma N \to \pi N$ for which Σ_{circ} vanishes. Since the soft-photon emission from the external charged particles does not contribute to Σ_{circ}, this observable acts as a filter to enhance the Δ-resonant process. Indeed, one observes from Fig. 14 that in the forward and upper quadrant (for $\Phi_\gamma > 0$) and at an energy $E'_\gamma = 100$ MeV, Σ_{circ} changes from 0 to -0.3 when κ_{Δ^+} is varied between 0 and 6. Furthermore, in the backward and upper quadrant and at an energy $E'_\gamma = 100$ MeV, Σ_{circ} changes between +0.15 and -0.05 when varying κ_{Δ^+} between 0 and 6. Since circularly polarized photons are readily available at MAMI, a measurement of Σ_{circ} for the $\gamma p \to \gamma \pi^0 p$ reaction in the $\Delta(1232)$ region provides a unique opportunity to enhance the Δ-resonant process and access κ_{Δ^+}.

We next investigate double spin observables where both the incident photon and the target proton are polarized. In Figs. 15 and 16 we display the sensitivity of the total helicity cross sections for the $\gamma p \to \gamma \pi^0 p$ reaction to the value of κ_{Δ^+}. Figure 15 shows the dependence of these cross sections on the outgoing photon energy, and Fig. 16 shows the pion angular distributions. These helicity cross sections are accessible experimentally by measuring the $\gamma p \to \gamma \pi^0 p$ reaction with a circularly polarized photon beam and a longitudinally polarized proton target, for the cases of parallel ($\sigma_{3/2}$) or antiparallel ($\sigma_{1/2}$) spins. It can be seen from Fig. 15 that in the low-energy limit ($E'_\gamma \to 0$), one exactly recovers

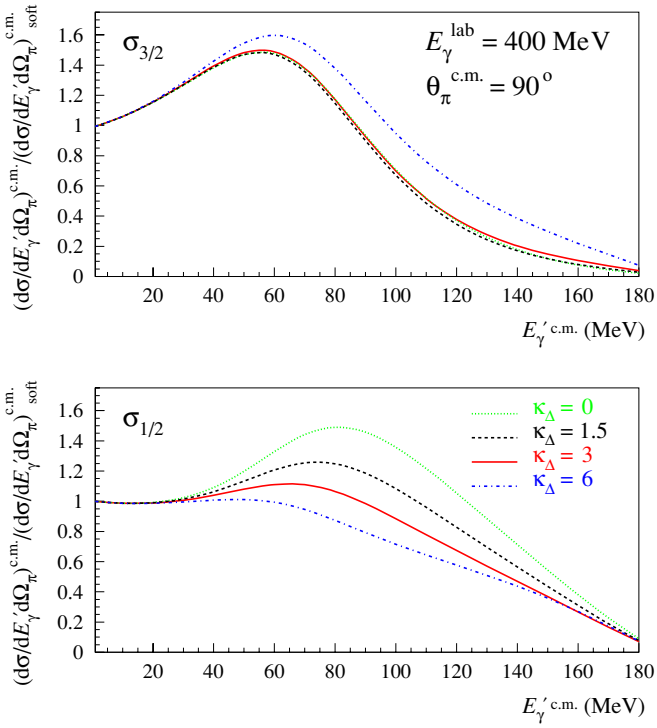

FIG. 15. (Color online) The helicity dependence of the $\gamma p \to \gamma \pi^0 p$ c.m. cross-section $d\sigma/dE'_\gamma d\Omega_\pi$, divided by its soft-photon value, as a function of the outgoing photon energy $E'^{\text{c.m.}}_\gamma$, at incident photon *lab* energy $E^{\text{lab}}_\gamma = 400$ MeV and pion emission angle $\theta^{\text{c.m.}}_\pi = 90^\circ$. Upper (lower) panel shows the cross sections for total helicity 3/2 (1/2). The curves correspond with the predictions of the unitary model for different values of κ_{Δ^+} as indicated on the figure.

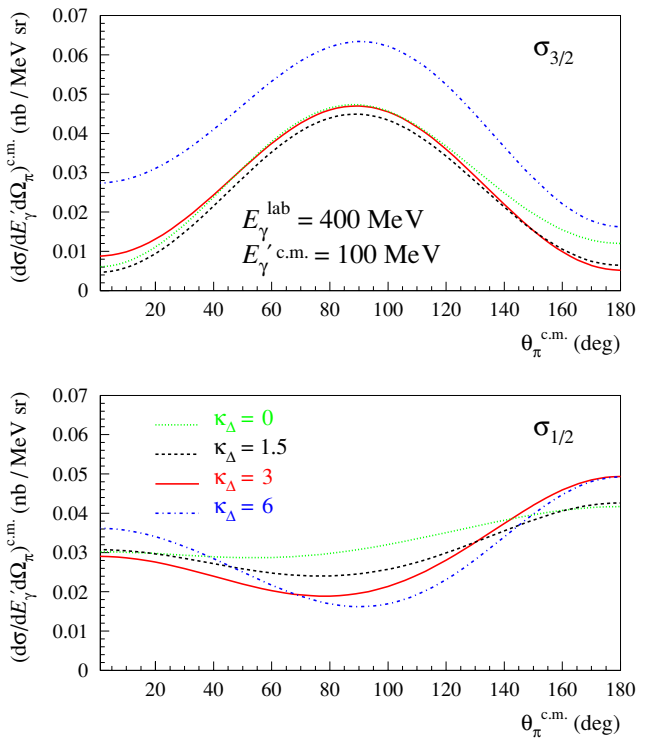

FIG. 16. (Color online) The angular dependence of the emitted pions for the $\gamma p \to \gamma \pi^0 p$ c.m. helicity cross-section $d\sigma/dE'_\gamma d\Omega_\pi$, at incident photon lab energy $E^{\text{lab}}_\gamma = 400$ MeV and fixed outgoing photon energy $E'^{\text{c.m.}}_\gamma = 100$ MeV. Upper (lower) panel shows the cross sections for total helicity 3/2 (1/2). The curves correspond with the predictions of the unitary model for different values of κ_{Δ^+} as indicated on the figure.

the helicity cross sections of the $\gamma p \to \pi^0 p$ reaction, for which we obtained a good description (see Fig. 6). At the higher values of E'_γ, one notices an interference pattern in the $\sigma_{3/2}$ cross section that strongly reduces the dependence on κ_{Δ^+} in the range from 0 to 3. The $\sigma_{1/2}$ cross section, on the other hand, decreases monotonically with increasing κ_{Δ^+}, thus indicating a very strong sensitivity to the Δ^+ MDM in the range 70 MeV $\leqslant E'_\gamma \leqslant$ 120 MeV (see Fig. 15, bottom). Also, the angular distribution of $\sigma_{1/2}$ is very sensitive to the value of κ_{Δ^+}, showing a rather flat distribution for $\kappa_{\Delta^+} = 0$ and a distinct minimum for $\kappa_{\Delta^+} = 6$ (see Fig. 16, bottom). A measurement of these helicity cross sections will be feasible in the near future at MAMI.

Although the main focus of our work is a unitary model for the $\gamma p \to \gamma \pi^0 p$ reaction in the $\Delta(1232)$-resonance region, we also obtain, within the same framework, a description of the $\gamma p \to \gamma \pi^+ n$ reaction. The tree-level part will now contain additional terms where the soft-photon couples to the charged pion as shown in Fig. 8. The rescattering terms in the soft-photon limit for $\gamma p \to \gamma \pi^+ n$ are obtained by the replacement $p' \to q$ in the second term of Eq. (27). As we have seen from the results in Sec. III, the $\gamma p \to \pi^+ n$ reaction has a much larger nonresonant contribution compared with the $\gamma p \to \pi^0 p$ reaction. For extracting information on the Δ^+ MDM, the $\gamma p \to \gamma \pi^0 p$ reaction is therefore clearly the favorite channel. However, the present experiments of Ref. [11] will simultaneously measure both $\gamma p \to \gamma \pi^0 p$ and $\gamma p \to \gamma \pi^+ n$ reactions. Therefore, the $\gamma p \to \gamma \pi^+ n$ data may provide a useful additional cross-check for our theoretical description. In Fig. 17, we show the outgoing photon energy dependence of the cross-section $d\sigma/dE'_\gamma$ for the $\gamma p \to \gamma \pi^+ n$ reaction, integrated over the photon and pion angles for three incoming photon energies through the $\Delta(1232)$ region. By comparing the left panels of Figs. 10 and 17, we observe that at small outgoing photon energies, the $\gamma p \to \gamma \pi^+ n$ cross sections are about a factor of 10 larger than the corresponding $\gamma p \to \gamma \pi^0 p$ cross sections. This is readily understood by the fact that in the soft-photon limit there is a large contribution due to radiation from the charged pion for the $\gamma p \to \gamma \pi^+ n$ process. On the other hand, for the $\gamma p \to \gamma \pi^0 p$ process only bremsstrahlung contributions arise from the emission of soft photons from the (much heavier) protons.

Similar to what we did in Fig. 10, we can also construct the ratio R between the $\gamma p \to \gamma \pi^+ n$ process and its soft-photon limit as given by the LET, which is derived in the Appendix, Sec. B [see Eq. (A16)]. In contrast to the $\gamma p \to \gamma \pi^0 p$ process, where this ratio shows clear resonance structure when increasing the final photon energy, the corresponding ratio for the $\gamma p \to \gamma \pi^+ n$ process drops monotonously with increasing E'_γ.

In Fig. 18, we show the pion angular dependence of the threefold differential cross section and photon asymmetry

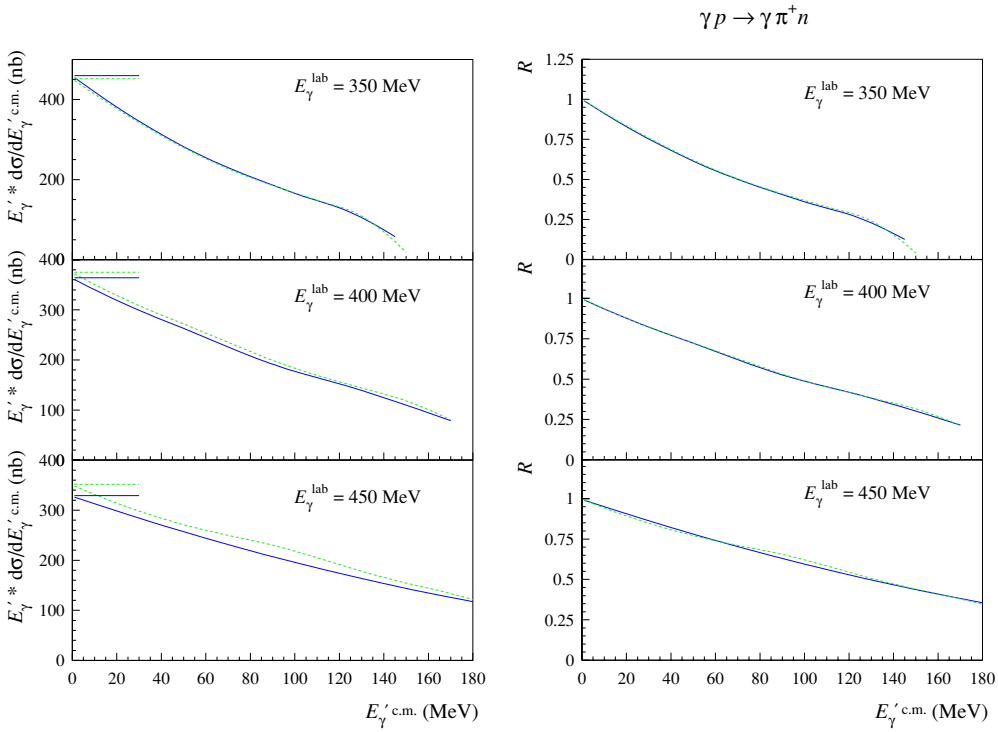

FIG. 17. (Color online) Left panel: outgoing photon energy dependence of the $\gamma p \to \gamma \pi^+ n$ cross-section $d\sigma/dE_\gamma^{\prime \mathrm{c.m.}}$ multiplied by $E_\gamma^{\prime \mathrm{c.m.}}$. Right panel: ratio R of the $\gamma p \to \gamma \pi^+ n$ process, as defined in Eq. (A16). Notation as in Fig. 10.

for the $\gamma p \to \gamma \pi^+ n$ reaction at $E_\gamma = 400$ MeV and $E'_\gamma = 100$ MeV. It can be seen from Fig. 18 that for an energy above the $\Delta(1232)$-resonance position, the $\gamma p \to \gamma \pi^+ n$ differential cross section exhibits a forward peaking analogous to the $\gamma p \to \pi^+ n$ process. Furthermore, it can be seen that both the differential cross section and the photon asymmetry for the $\gamma p \to \gamma \pi^+ n$ reaction only display a rather modest change when varying κ_{Δ^+} between 0 and 6. Therefore, the measurement of the $\gamma p \to \gamma \pi^+ n$ process can put stringent constraints on our theoretical description of the nonresonant contributions, making it a useful tool to minimize model dependencies when extracting information on the Δ^+ MDM from the $\gamma p \to \gamma \pi^0 p$ process.

VI. CONCLUSIONS AND OUTLOOK

In this work, we provided a unitary model for the $\gamma p \to \gamma \pi N$ reaction in the $\Delta(1232)$ region. Our starting point is a unitary model for the $\gamma p \to \pi N$ ($\pi N = \pi^0 p, \pi^+ n$) reaction based on a transition potential consisting of Born diagrams, vector meson exchanges, and Δ-resonant process. The rescattering effects are included in an onshell (K-matrix) approximation. Besides the vector meson coupling constants, the only free parameters in this model are the $\gamma N \Delta$ electric and magnetic couplings. With this model we find a very reasonable description of both total unpolarized and helicity cross sections as well as differential cross sections and photon asymmetries for both the $\gamma p \to \pi^0 p$ and $\gamma p \to \pi^+ n$ processes through the $\Delta(1232)$-resonance region.

The model for the $\gamma p \to \pi N$ processes was then extended to describe the $\gamma p \to \gamma \pi N$ reactions. Our model for these reactions is gauge invariant with respect to both initial and final photons. In particular, it is constructed such that in the limit of small outgoing photon energy, it exactly reproduces the low-energy theorem that relates the $\gamma p \to \gamma \pi N$ and $\gamma p \to \pi N$ processes. For the $\gamma p \to \gamma \pi N$ reactions, the tree-level terms include Born diagrams, vector meson exchanges, the $\pi^0 \to \gamma\gamma$ anomaly contribution, and the $\Delta(1232)$ contribution. The rescattering effects are calculated in the soft-photon approximation using the previously described model for $\gamma p \to \pi N$. In this framework, the only new parameter entering in to the description of the $\gamma p \to \gamma \pi N$ process is the $\Delta^+(1232)$ magnetic dipole moment (MDM).

Using this unitary model, we investigated several $\gamma p \to \gamma \pi N$ observables. We found good agreement for the existing experimental data of the $\gamma p \to \gamma \pi^0 p$ reaction. In particular, the rescattering effects were found to slightly reduce the cross sections at the larger outgoing photon energies, which improved the agreement with the data. We then studied the sensitivity of the $\gamma p \to \gamma \pi^0 p$ observables to the Δ^+ MDM. The unpolarized differential cross section displays an interference structure which reduces the sensitivity to values of κ_{Δ^+} in the range between 0 and 3. However, the photon asymmetry for linearly polarized incident photons is strongly dependent on κ_{Δ^+}, and it changes between 0.35 and 0.15 when κ_{Δ^+} is varied between 0 and 6. The dedicated measurements of the photon asymmetry that are currently underway at MAMI are therefore highly promising for a more quantitative extraction of the Δ^+ MDM.

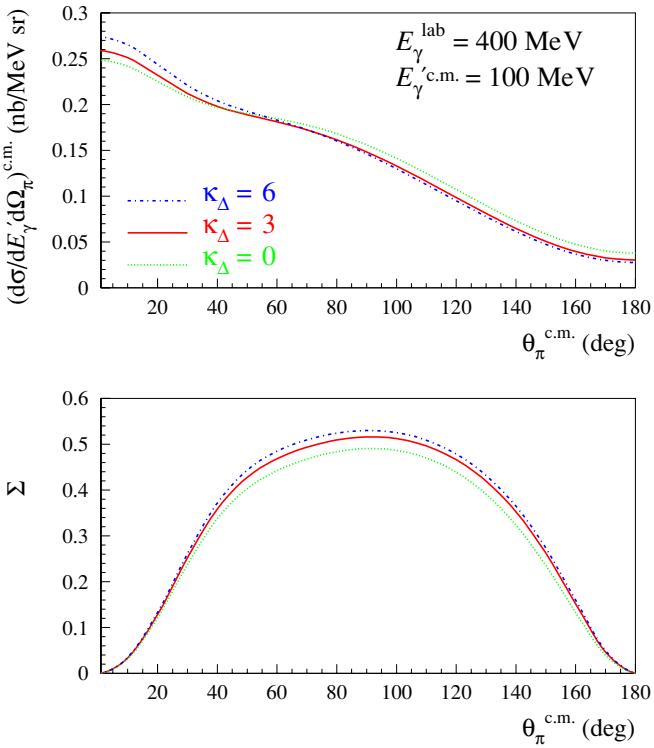

FIG. 18. (Color online) Top: the angular distribution of the emitted pions for the $\gamma p \to \gamma \pi^+ p$ threefold differential c.m. cross-section $d\sigma/dE_\gamma' d\Omega_\pi$ at incident photon lab energy $E_\gamma^{\rm lab} = 400$ MeV and fixed outgoing photon energy $E_\gamma'^{\rm c.m.} = 100$ MeV. The sensitivity of the unitary model to different values of κ_{Δ^+} is shown. Bottom: same for the photon asymmetry Σ.

The single asymmetry for circularly polarized incident photons provides a new observable for a three-body reaction such as $\gamma p \to \gamma \pi N$ if the photon is emitted out of the plane defined by the incident photon and the final pion. This asymmetry has the interesting feature that it vanishes exactly in the soft-photon limit, where the $\gamma p \to \gamma \pi^0 p$ process effectively reduces to a two-body reaction, for which the asymmetry vanishes. Since the pure bremsstrahlung due to soft-photon emission from the external charged particles does not contribute, the single asymmetry for circularly polarized incident photons therefore acts as a filter to enhance the Δ-resonant process, and indeed our results display a strong sensitivity to the Δ^+ MDM.

Yet another sensitive observable with regard to the Δ^+ MDM is the helicity cross section $\sigma_{1/2}$. In particular, this differential cross section changes by about a factor of 2 when κ_{Δ^+} is varied between 0 and 6.

Besides a prediction for the $\gamma p \to \gamma \pi^0 p$ observables, our unitary model also provides a description of the $\gamma p \to \gamma \pi^+ n$ reaction. However, the $\gamma p \to \gamma \pi^+ n$ process is dominated by nonresonant processes and bremsstrahlung contributions originating from radiation off the charged pion line. Therefore, the measurement of the $\gamma p \to \gamma \pi^+ n$ process will put stringent constraints on our theoretical description of the nonresonant contributions and can be useful in minimizing model dependencies when extracting information on the Δ^+ MDM from the $\gamma p \to \gamma \pi^0 p$ process.

To improve on the accuracy in the extraction of the Δ^+ MDM, the present framework may be extended to include the rescattering corrections at finite final photon energies. At such energies the final photon can be emitted not only from the external charged lines, as in Figs. 9(b) and (c), but also from an intermediate line. A particularly important contribution in the Δ region is expected to come from the $\Delta \to \pi N \to \Delta$ self-energy where the photon is emitted from the light pion in the loop. The Ward identity then requires that the energy dependence of this vertex correction be consistent with the energy dependence of the Δ self-energy. Such a calculation, which will provide an imaginary part to the $\gamma \Delta \Delta$ vertex, is beyond the scope of the present work (see, e.g., Ref. [35] where it has been evaluated for the $\pi N \to \pi N \gamma$ reaction). Its evaluation for the $\gamma N \to \gamma \pi N$ reaction is left for a future work [36] and will serve as an input in the present framework in order to extend its range of applicability.

The upcoming dedicated measurements of the $\gamma p \to \gamma \pi N$ reaction will certainly trigger new theoretical efforts with the aim to further minimize the model dependencies in the extraction of the Δ^+ MDM.

ACKNOWLEDGMENTS

The authors would like to thank R. Beck, M. Kotulla, and V. Pascalutsa for helpful discussions. W.-T. C. is grateful to the Universität Mainz for the hospitality extended to him during his visits. This work was supported in part by the National Science Council of ROC under grant Nos. NSC92-2112-M002-013 and NSC92-2112-M-001-058, the Deutsche Forschungsgemeinschaft (SFB 443), a joint project NSC/DFG TAI-113/10/0, and the U.S. Department of Energy under contracts DE-FG02-04ER41302 and DE-AC05-84ER40150.

APPENDIX: DERIVATION OF THE LOW-ENERGY THEOREMS

A. Low-energy theorem relating the $\gamma p \to \gamma \pi^0 p$ and $\gamma p \to \pi^0 p$ processes

In the soft-photon limit the $\gamma p \to \gamma \pi^0 p$ reaction is exactly described by the bremsstrahlung process from the initial and final protons. This yields the fivefold differential c.m. cross section in the limit $k' \to 0$ of

$$\left(\frac{d\sigma}{dE_\gamma' d\Omega_\pi d\Omega_\gamma}\right)^{\rm c.m.} \longrightarrow \frac{e^2}{16\pi^3} E_\gamma' \sum_{\lambda'} \times \left| \frac{p' \cdot \varepsilon(k', \lambda')}{p' \cdot k'} - \frac{p \cdot \varepsilon(k', \lambda')}{p \cdot k'} \right|^2 \left(\frac{d\sigma}{d\Omega_\pi}\right)^{\rm c.m.}, \quad \text{(A1)}$$

where $(d\sigma/d\Omega_\pi)^{\rm c.m.}$ is the c.m. cross section for the $\gamma p \to \pi^0 p$ process, $\lambda' = \pm 1$ the photon polarization, and ε its polarization vector. We calculate the rhs of Eq. (A1) by performing the sum over the photon polarizations and integrating over the

photon angles. This gives

$$\left(\frac{d\sigma}{dE'_\gamma d\Omega_\pi}\right)^{\text{c.m.}} \longrightarrow \frac{e^2}{16\pi^3}\, E'_\gamma\, \mathcal{I} \left(\frac{d\sigma}{d\Omega_\pi}\right)^{\text{c.m.}}, \qquad \text{(A2)}$$

where we introduced the photon angular integral $\mathcal{I}$ as

$$\mathcal{I} \equiv \int d\Omega_\gamma^{\text{c.m.}} \left[\frac{2p\cdot p'}{(p\cdot k')(p'\cdot k')} - \frac{M_N^2}{(p\cdot k')^2} - \frac{M_N^2}{(p'\cdot k')^2}\right]. \qquad \text{(A3)}$$

In Eq. (A3), the second and third terms arise from the contribution of bremsstrahlung from the initial and final proton, respectively, whereas the first term stems from the interference between the bremsstrahlung amplitudes from the initial and final protons.

We next work out the photon angular integral of Eq. (A3). It is convenient to introduce the initial and final nucleon velocities $\boldsymbol{\beta_N} \equiv \boldsymbol{p}/E_N$ and $\boldsymbol{\beta'_N} \equiv \boldsymbol{p'}/E'_N$, and a Feynman parametrization of the first term of Eq. (A3), which brings the propagators to the same denominator. The result is

$$\begin{aligned}\mathcal{I} = \frac{2\pi}{(E'_\gamma)^2}\Bigg\{&(1-\boldsymbol{\beta_N}\cdot\boldsymbol{\beta'_N})\int_{-1}^{+1} dy \int_{-1}^{+1} dx\, \frac{1}{(1-\beta_y x)^2}\\ &-\left(1-\beta_N^2\right)\int_{-1}^{+1} dx\, \frac{1}{(1-\beta_N x)^2}\\ &-\left(1-\beta_N'^2\right)\int_{-1}^{+1} dx\, \frac{1}{(1-\beta'_N x)^2}\Bigg\}, \end{aligned} \qquad \text{(A4)}$$

where β_N, β'_N, and β_y are the magnitudes of $\boldsymbol{\beta_N}$, $\boldsymbol{\beta'_N}$, and $\boldsymbol{\beta_y}$, which are related by

$$\boldsymbol{\beta_y} \equiv \boldsymbol{\beta_N}\,\frac{1}{2}(1+y) + \boldsymbol{\beta'_N}\,\frac{1}{2}(1-y). \qquad \text{(A5)}$$

By use of the identity

$$\int_{-1}^{+1} dx\, \frac{1}{(1-\beta x)^2} = \frac{2}{1-\beta^2}, \qquad \text{(A6)}$$

Eq. (A4) can be cast into the form

$$\mathcal{I} = \frac{2\pi}{(E'_\gamma)^2}\left\{-4 + 2\,(1-\boldsymbol{\beta_N}\cdot\boldsymbol{\beta'_N})\int_{-1}^{+1} dy\, \frac{1}{\left(1-\beta_y^2\right)}\right\}. \qquad \text{(A7)}$$

We next define the variable

$$v \equiv \sqrt{1+\frac{4M_N^2}{-t}}, \qquad \text{(A8)}$$

with $t = (p'-p)^2$. This allows us to derive the relations

$$(1-\boldsymbol{\beta_N}\cdot\boldsymbol{\beta'_N}) = \left(1-\beta_N^2\right)^{1/2}\left(1-\beta_N'^2\right)^{1/2}\left(\frac{v^2+1}{v^2-1}\right) \qquad \text{(A9)}$$

and

$$\begin{aligned}\int_{-1}^{+1} dy \frac{1}{\left(1-\beta_y^2\right)} = &\frac{1}{\left(1-\beta_N^2\right)^{1/2}\left(1-\beta_N'^2\right)^{1/2}}\\ &\cdot\left(\frac{v^2-1}{2v}\right)\ln\left(\frac{v+1}{v-1}\right)^2. \end{aligned} \qquad \text{(A10)}$$

Combining Eqs. (A6–A10), we finally obtain

$$\mathcal{I} = \frac{8\pi}{(E'_\gamma)^2}\left[-1+\left(\frac{v^2+1}{2v}\right)\cdot\ln\left(\frac{v+1}{v-1}\right)\right]. \qquad \text{(A11)}$$

If we insert this expression into the soft-photon limit for the cross section of Eq. (A2), Eq. (32) follows immediately.

B. Low-energy theorem relating the $\gamma p \to \gamma\pi^+ n$ and $\gamma p \to \pi^+ n$ processes

The low-energy limit of π^+ production may be derived from the previous results by a simple consideration. Whereas in the case of π^0 production all final-state radiation comes from the protons, in the case of π^+ production the charged pion in the final state will radiate. Hence we obtain the relevant photon angular integral from $\mathcal{I}$ of Eq. (A3) by replacing $p' \to q$ and, in the third term, $M_N^2 \to m_\pi^2$. The result is

$$\left(\frac{d\sigma}{dE'_\gamma d\Omega_\pi}\right)^{\text{c.m.}} \longrightarrow \frac{e^2}{16\pi^3}\, E'_\gamma\, \tilde{\mathcal{I}} \left(\frac{d\sigma}{d\Omega_\pi}\right)^{\text{c.m.}}, \qquad \text{(A12)}$$

with

$$\tilde{\mathcal{I}} \equiv \int d\Omega_\gamma^{\text{c.m.}} \left[\frac{2p\cdot q}{(p\cdot k')(q\cdot k')} - \frac{M_N^2}{(p\cdot k')^2} - \frac{m_\pi^2}{(q\cdot k')^2}\right], \qquad \text{(A13)}$$

where the second and third terms arise from the contribution of bremsstrahlung from the initial proton and final pion alone, whereas the first term stems from the interference between the bremsstrahlung amplitudes from the initial proton and the final pion.

We next work out the photon angular integral of Eq. (A13) along the same lines as in the case of a neutral pion. We introduce the initial nucleon velocity $\boldsymbol{\beta_N} \equiv \boldsymbol{p}/E_N$ and the final pion velocity $\boldsymbol{\beta_\pi} \equiv \boldsymbol{q}/\omega_\pi$, define an appropriate variable $\tilde{v}$ as

$$\tilde{v} \equiv \sqrt{1+\frac{4M_N m_\pi}{(M_N-m_\pi)^2-u}}, \qquad \text{(A14)}$$

where $u \equiv (p-q)^2$. The bremsstrahlung integral of Eq. (A13) can then be worked out analogously as in Eq. (A11) and yields

$$\tilde{\mathcal{I}} = \frac{8\pi}{(E'_\gamma)^2}\left[-1+\left(\frac{\tilde{v}^2+1}{2\tilde{v}}\right)\ln\left(\frac{\tilde{v}+1}{\tilde{v}-1}\right)\right]. \qquad \text{(A15)}$$

We note as an additional check that the new variable $\tilde{v}$ turns into the previous variable v if we replace $m_\pi \to M_N$ and $q \to p'$.

Finally, we can also introduce the ratio R between the $\gamma p \to \gamma\pi^+ p$ process in the limit of a soft outgoing photon and the $\gamma p \to \pi^+ n$ process as

$$R \equiv \frac{1}{\sigma_{\pi^+}}\cdot E'_\gamma \frac{d\sigma}{dE'_\gamma} \to 1 \quad \text{for } E'_\gamma \to 0, \qquad \text{(A16)}$$

with σ_{π^+} defined as

$$\sigma_{\pi^+} \equiv \frac{e^2}{2\pi^2}\int d\Omega_\pi^{\text{c.m.}}\, W(\tilde{v}) \left(\frac{d\sigma}{d\Omega_\pi}\right)^{\text{c.m.}}. \qquad \text{(A17)}$$

In Eq. (A17), $W(\tilde{v})$ is obtained from Eq. (31) by making the replacement $v \to \tilde{v}$.

[1] G. Blanpied *et al*., Phys. Rev. C **64**, 025203 (2001).
[2] S. N. Yang and S. S. Kamalov, Mod. Phys. Lett. **A18**, 248 (2003); S. S. Kamalov, S. N. Yang, D. Drechsel, O. Hanstein, and L. Tiator, Phys. Rev. C **64**, 032201 (2001).
[3] T. M. Aliev, A. Özpineci, and M. Savci, Nucl. Phys. **A678**, 443 (2000).
[4] D. B. Leinweber, T. Draper, and R. M. Woloshyn, Phys. Rev. D **46**, 3067 (1992).
[5] I. C. Cloet, D. B. Leinweber, and A. W. Thomas, Phys. Lett. **B563**, 157 (2003).
[6] B. M. K. Nefkens *et al*., Phys. Rev. D **18**, 3911 (1978).
[7] A. Bosshard *et al*., Phys. Rev. D **44**, 1962 (1991).
[8] K. Hagiwara *et al*. (Particle Data Group), Phys. Rev. D **66**, 010001 (2002).
[9] M. M. Giannini, in *Proceedings of the Workshop on Perspectives on Nuclear Physics at Intermediate Energies, ICTP, Trieste, Italy, 1983* (World Scientific, Singapore, 1984); D. Drechsel, in MAMI funding proposal to DFG, SFB 201 (1984–86), p. 56.
[10] M. Kotulla *et al*., Phys. Rev. Lett. **89**, 272001 (2002).
[11] R. Beck and B. Nefkens, spokespersons, Crystal Ball @ MAMI experiment.
[12] A. I. Machavariani, A. Faessler, and A. J. Buchmann, Nucl. Phys. **A646**, 231 (1999); Nucl. Phys. **A686**, 601 (E) (2001).
[13] D. Drechsel, M. Vanderhaeghen, M. M. Giannini, and E. Santopinto, Phys. Lett. **B484**, 236 (2000).
[14] D. Drechsel and M. Vanderhaeghen, Phys. Rev. C **64**, 065202 (2001).
[15] S. N. Yang, Chin. J. Phys. **29**, 485 (1991).
[16] D. Drechsel, O. Hanstein, S. Kamalov, and L. Tiator, Nucl. Phys. **A645**, 145 (1999).
[17] S. N. Yang, J. Phys. G **11**, L205 (1985).
[18] J. Hamilton and W. S. Woolcock, Rev. Mod. Phys. **35**, 737 (1960).
[19] S. S. Kamalov and S. N. Yang, Phys. Rev. Lett. **83**, 4494 (1999).
[20] S. S. Hsiao, C. T. Hung, J. L. Tsai, S. N. Yang, and Y. B. Dong, Few-Body Syst. **25**, 25 (1998).
[21] H. Tanabe and K. Ohta, Phys. Rev. C **31**, 1876 (1985).
[22] M. El Amiri, G. López Castro, and J. Pestieau, Nucl. Phys. **A543**, 673 (1992).
[23] M. MacCormick *et al*., Phys. Rev. C **53**, 41 (1996).
[24] J. Ahrens *et al*., Phys. Rev. Lett. **84**, 5950 (2000).
[25] D. A. McPherson *et al*., Phys. Rev. **136**, B1465 (1964).
[26] K. G. Fissum *et al*., Phys. Rev. C **53**, 1278 (1996).
[27] H. Genzel *et al*., Z. Phys. **268**, 43 (1974).
[28] R. Beck *et al*., Phys. Rev. C **61**, 035204 (2000).
[29] G. López Castro and A. Mariano, Nucl. Phys. **A697**, 440 (2002).
[30] R. A. Arndt, W. J. Briscoe, I. I. Strakovsky, and R. L. Workman, Phys. Rev. C **66**, 055213 (2002).
[31] J. Wess and B. Zumino, Phys. Lett. **B37**, 95 (1971).
[32] S. Weinberg, in *Lectures on Elementary Particles and Quantum Field Theory*, Vol. 1, Brandeis University Summer Institute 1970, edited by S. Deser, M. Grisaru, and H. Pendleton (MIT Press, Cambridge, MA, 1970).
[33] S. Ferrara, M. Porrati, and V. L. Telegdi, Phys. Rev. D **46**, 3529 (1992).
[34] W.-T. Chiang, S. N. Yang, M. Vanderhaeghen, and D. Drechsel, Nucl. Phys. **A723**, 205 (2003).
[35] L. Heller, S. Kumano, J. C. Martinez, and E. J. Moniz, Phys. Rev. C **35**, 35 (1987).
[36] V. Pascalutsa and M. Vanderhaeghen, nucl-th/0412113 (to be published).